

Prepared in cooperation with the U.S. Environmental Protection Agency and the Washington State Department of Ecology

BFS—A Non-Linear, State-Space Model for Baseflow Separation and Prediction

Scientific Investigations Report 2022–5114

BFS—A Non-Linear, State-Space Model for Baseflow Separation and Prediction

By Christopher P. Konrad

Prepared in cooperation with the U.S. Environmental Protection Agency and the
Washington State Department of Ecology

Scientific Investigations Report 2022–5114

U.S. Geological Survey, Reston, Virginia: 2022

For more information on the USGS—the Federal source for science about the Earth, its natural and living resources, natural hazards, and the environment—visit <https://www.usgs.gov> or call 1–888–ASK–USGS.

For an overview of USGS information products, including maps, imagery, and publications, visit <https://store.usgs.gov/>.

Any use of trade, firm, or product names is for descriptive purposes only and does not imply endorsement by the U.S. Government.

Although this information product, for the most part, is in the public domain, it also may contain copyrighted materials as noted in the text. Permission to reproduce copyrighted items must be secured from the copyright owner.

Suggested citation:

Konrad, C.P., 2022, BFS—A non-linear, state-space model for baseflow separation and prediction: U.S. Geological Survey Scientific Investigations Report 2022–5114, 24 p., <https://doi.org/10.3133/sir20225114>.

Associated data for this publication:

Konrad, C.P., 2020, Non-linear baseflow separation model with parameters and results (ver. 2.0, October 2022) : U.S. Geological Survey data release, <https://doi.org/10.5066/P9AIPHEP>.

ISSN 2328-0328 (online)

Acknowledgments

Development of the baseflow separation model was supported by the U.S. Environmental Protection Agency National Estuary Program and the U.S. Geological Survey Water Availability and Use Science Program. Jeff Marti, Washington State Department of Ecology, provided useful suggestions for improving the forecasting capability of the model.

Contents

Acknowledgments	iii
Abstract	1
Introduction.....	2
Purpose and Scope	2
State-Space Baseflow Models	2
Hydrograph Separation	2
Model Description	3
Conceptual Stream Basin and Flow System	4
Relation of Surface-Reservoir Storage to Saturated Thickness	5
Relations of Base-Reservoir Storage and Saturated Thickness	5
Storage-Discharge Relations for Surface and Base Reservoirs	7
Water Balance	8
Impulses, Direct Runoff, Infiltration, and Recharge.....	8
Model Implementation	9
Model Parameters	9
Order of Calculations.....	11
Initial Conditions	12
Estimates at the Beginning of a Time Step	12
Estimates at the End of the Time Step	12
Model Error	12
Model Output.....	13
Model Calibration.....	14
Step 1. Initial Calibration with Fixed Parameters for the Base Reservoir	15
Step 2. Calibration of Storage-Discharge Relation for the Base Reservoir	15
Steps 3 and 4. Calibration of bf_sep for Baseflow Error and Total Error	16
Calibration of Multiple Sites.....	16
Base-Flow Simulations	16
Comparison of Base-Flow Simulation to Graphical Hydrograph Separation	19
Low-Flow Prediction and Forecasting	20
Summary.....	22
References Cited.....	23

Figures

1. Block diagram showing oblique view of the conceptual stream basin with a longitudinal section of the surface reservoir showing its saturated thickness, Z_{sr} at the point where the water surface intersects the land surface and longitudinal section of the base reservoir (right image) with its saturated thickness, Z_{br} at the point where its water surface intersects the channel, X_b4
2. Examples of longitudinal sections of reservoirs with parameters for equation 4—a reservoir with a triangular longitudinal section; moderately curved longitudinal section; and highly curved longitudinal section; storage, discharge, ratio of discharge to storage for the triangular and moderately curved longitudinal sections using additional parameters; and discharge-to-storage ratio is constant with storage for linear first-order recession.....6

3.	Map of the United States with the simulated baseflow fraction for 13,208 sites where the baseflow separation model was calibrated.....	17
4.	Hydrographs showing observed daily streamflow, simulated baseflow, and the sum of simulated surface and baseflow calibrated model output for the North Fork Stillaguamish River, water years 2014–15.....	18
5.	Scatterplot showing comparison of the baseflow index to the simulated baseflow fraction of streamflow for 8,368 sites with streamgages operated by the U.S. Geological Survey.....	19
6.	Graph showing difference between baseflow fraction and baseflow index in relation to basin area	19
7.	Difference between baseflow fraction and baseflow index in relation to reservoir storage for 7,461 sites where data are available	20
8.	Difference between baseflow fraction and baseflow index in relation to mean basin elevation for 5,794 sites where upstream reservoir storage is less than 100 days of mean streamflow	20
9.	Map showing median annual absolute fractional error for streamflow on the day of the annual longest recession period at 13,208 sites.....	21
10.	Graph showing median annual simulated streamflow plus precision as a fraction of measured streamflow plus precision on the last day of annual longest recession plotted against the length of the recession period at 7,546 sites with at least 10 years of daily streamflow record where reservoir storage is less than 100 days of mean streamflow and the median annual longest recession period is at least 10 days	22

Tables

1.	Flux calculations.....	5
2.	Description of functions used for the baseflow separation model.....	7
3.	Parameters describing streamflow characteristics in the vector <i>flow</i> used as an argument in the function <i>bf_sep</i>	9
4.	Parameters defining the geometry of the stream basin in the vector <i>basin_char</i> used as an argument to the function <i>bf_sep</i>	10
5.	Hydraulic parameters in the vector <i>gw_hyd</i> used as an argument to the function <i>bf_sep</i>	11
6.	Description of model output, <i>bf_mod_out</i>	14
7.	Calibration functions for baseflow separation model	15

Conversion Factors

U.S. customary units to International System of Units

Multiply	By	To obtain
	Flow rate	
cubic foot per second (ft ³ /s)	0.02832	cubic meter per second (m ³ /s)

International System of Units to U(6).S. customary units

Multiply	By	To obtain
	Length	
meter (m)	3.281	foot (ft)
	Area	
square kilometer (km ²)	0.3861	square mile (mi ²)
	Flow rate	
cubic meter per second (m ³ /s)	35.31	cubic foot per second (ft ³ /s)

Datum

Horizontal coordinate information is referenced to the North American Datum of 1983 (NAD 83).

Definitions of Terms

Model. A conceptual or quantitative representation of hydrologic fluxes and states.

Algorithm. A series of calculations or logical tests used for a quantitative solution to a problem used to determine the value of a variable in a model.

Function. An equation that relates one variable to one or more other variables; a series of commands in R that are run using a text string with additional arguments in ().

Argument. The variables needed to run a function in R; an argument can be a single variable or a vector of multiple variables.

Parameter. A variable with a constant at-a-site value used in a function.

R functions, arguments, and parameters are *italicized* in the text.

Time-series variables, which vary over time, are noted by (t).

Abbreviations

BFF	baseflow fraction
BFI	baseflow index
BFS	baseflow separation
CONUS	continental United States
L	length dimension
L3	volume dimension
NA	not available
NWIS	National Water Information System
SFF	surface flow fraction
USGS	U.S. Geological Survey

BFS—A Non-Linear, State-Space Model for Baseflow Separation and Prediction

By Christopher P. Konrad

Abstract

Streamflow in rivers can be separated into a relatively steady component, or baseflow, that represents reliably available surface water and more dynamic components of runoff that typically represent a large fraction of total streamflow. A spatially aggregated numerical time-series model was developed to separate the baseflow component of a streamflow time-series using a state-space framework in which baseflow is a non-linear function of upstream storage, an unmeasured state variable. The state-space framework allows forecasting of baseflow for periods with no rainfall or snowmelt and estimation of residence times in contrast to other hydrograph separation models. The use of a non-linear relation between baseflow and storage maintains model performance over a wide range of time scales but will only provide reliable predictions for periods when the rate of streamflow recession as a fraction of streamflow decreases over time.

The baseflow separation model, BFS, is implemented as set of functions in the statistical computing language R. BFS is run using the main function, *bf_sep*, which reads model input (a time series of streamflow), calculates the baseflow component of streamflow, writes model output to a file, and returns an error to the user to facilitate automated calibration. The function, *bf_sep*, has six arguments, which a user must enter: a numerical vector with the time series of measured streamflow volume for each time step; a character string, *timestep*, that has a value of either “daily” or “hourly” indicating the time step; a character string, *error_basis*, indicating which simulated streamflow components are used for error calculations; a six-element numeric vector, *flow*, with parameters characterizing streamflow; a six-element vector, *basin_char*, with parameters characterizing the geometry of stream basin and reservoirs; and a six-element vector, *gw_hyd*, with hydraulic parameters. The function *bf_sep* calls a series of other functions to calculate surface and base reservoir storage and fluxes.

Calibration of a non-linear model for baseflow recession must confront three issues. First, baseflow is a component of streamflow, so it is always less than or equal to streamflow but there is no independent standard for the baseflow component of streamflow. Second, optimization routines can converge on a set of model parameters that result in relatively steady but

minimal baseflow that does not exceed streamflow, Q , but has a limited dynamic range. Third, the power function used to generate non-linear first-order baseflow recession ($dQ/dt)/Q \neq \text{constant}$) may only be sensitive to parameters over a limited range of values, which may not be found by optimization routines.

To address these issues, BFS calculates error as the mean of weighted differences between measured streamflow and either simulated baseflow or the sum of simulated baseflow and surface flow as a fraction of measured streamflow. The difference for each time step is weighted by an exponential function of the length of recession for each time step ranging from 0 for periods when streamflow increases and approaching 1 for long recessional periods. The weight is set to 1 for any time step when simulated streamflow exceeds measured streamflow. Error calculation incorporates limited precision of streamflow measurements.

A four-step calibration process was developed to find a set of viable parameters that maximize the baseflow component within the constraints of the conceptual model (a first-order recession rate that decreases during dry periods). BFS was calibrated at 13,208 U.S. Geological Survey streamgages with available daily streamflow records for at least 300 days from water years 1981 to 2020. The total simulated baseflow component as a fraction of streamflow (BFF) was generally less than the baseflow index (BFI) for 8,368 streamgages where BFF and BFI were available. The median difference was $\text{BFF} - \text{BFI} = 0.11$. Large differences were most common in the Interior West where streamflow in many rivers is regulated and is generated predominantly by snowmelt. The baseflow separation model generally allocates less streamflow to baseflow than graphical hydrograph separation in snowmelt rivers.

BFS can be used to forecast streamflow during dry periods by using a time series of real-time streamflow with values of Not Available (NA), appended to the time-series to represent missing (future) streamflow values. The forecast skill of BFS was evaluated in terms of difference between simulated baseflow and measured streamflow as a fraction of measured streamflow on the days of the annual maximum recession period at 5,916 of the sites with at least 10 years of record. The median annual error was less than 50 percent at one-half of the sites and generally improved for drier years with longer recession periods.

Introduction

Many rivers and streams have a relatively steady component of streamflow, or baseflow, generated by groundwater discharge, meltwater from glaciers or snowfields, outflow from lakes and reservoirs, and routing of streamflow over long distances. Baseflow represents reliable water supply during dry periods for human use and aquatic habitats (Konrad, 2006a). Baseflow can have a physio-chemical signature (for example, specific conductance, dissolved constituents) that is distinct from quick-response runoff indicating difference in their sources (Miller and others, 2014). As a result, estimates of baseflow are important for assessing the availability of streamflow and aquatic habitats in rivers and streams during extended dry periods and attributing loads of dissolved materials to their sources (Mahler and others, 2021). Comparative analysis of baseflow across streams contributes to an understanding of regional hydrology and its heterogeneity in terms streamflow responses to precipitation (Curtis and others, 2020).

Purpose and Scope

A spatially aggregated, state-space numerical model for baseflow separation (BFS) was developed to estimate the baseflow component of a streamflow at a site with a daily streamflow record and to predict baseflow during dry periods. The state-space structure, in which baseflow is a function of the unmeasured aquifer storage, allows for baseflow prediction and is distinct from other hydrograph separation methods. This report documents the conceptual model for baseflow generation, the formulas used to calculate storage and fluxes while maintaining a water balance, and the implementation of BFS in terms of the order of calculations. The report also describes application of model including a parameter calibration procedure for low-flow estimation at 13,208 sites with at least 5 years of daily streamflow records from water years 1981 to 2020.

State-Space Baseflow Models

State-space models of baseflow, which relate aquifer storage to streamflow recession (Jakeman and others, 1990; Konrad, 2006a), offer the prospects of forecasting low flows in rivers and streams and accounting for groundwater residence times that affect source-water chemistry. State-space hydrologic models generally represent groundwater discharge, $Q(t)$, to rivers and streams as a linear function of aquifer storage, S (Dooge, 1959; Clark and others, 2008; Neitsch and others, 2011; Regan and others, 2018; Gochis and others, 2020). In these “linear reservoir” models, discharge from an aquifer to a river or stream decreases over time as a first-order linear function of discharge, $dQ/dt = RQ$, such that groundwater discharge over time, $Q(t)$, follows an exponential function:

$$Q(t) = Q_0 e^{t/\tau}, \quad (1)$$

where

$$\begin{array}{ll} Q_0 & \text{is discharge at any specified initial time,} \\ Q(t) & \text{is the discharge after time, } t, \text{ and} \\ \tau & \text{is the recession coefficient [1/T].} \end{array}$$

Linear recession of streamflow is consistent with groundwater discharge to a stream from an unconfined aquifer where the saturated thickness is uniform, the hydraulic gradient is constant, and discharge is a linear function of saturated thickness, which represents the Boussinesq equation under the Dupuit-Forchheimer assumptions (Freeze and Cherry, 1979). The aquifer must have a constant length and a constant width so that storage and discharge only depend on its saturated thickness.

Although models using first-order linear recession can reproduce the measured recession of streamflow over short-time scales (days), they are challenged by streamflow recession over longer time scales (weeks to months) (Konrad, 2006a). Streamflow can recess to a relatively steady baseflow (decreasing recession rate constant over time), where it is supported by discharge from an aquifer with a large spatial extent and high specific yield. Alternatively, streamflow recession can increase over time where groundwater storage is limited or where streams go dry when groundwater levels decline below the elevation of the streambed. Non-linear relations between groundwater storage and discharge (Wittenberg, 1999; Botter and others, 2009) become critical for simulating baseflow recession over time scales of weeks to months typical of extended drought (Tallaksen, 1995). Analytical solutions for non-linear forms of the Boussinesq equation have been developed by Serrano and Workman (1998) and Konrad (2006a) to account for time-varying transmissivity of unconfined aquifers interacting with rivers at short- and long-times scales, respectively.

A non-linear, unconfined aquifer that conforms to the Dupuit-Forchheimer assumptions (horizontal groundwater flow and discharge in proportion to saturated thickness) requires that either the effective length or width of the saturated thickness of the aquifer varies over time. In these cases, the change in water level will not be proportional to the de-watered volume as the aquifer drains, so discharge from the aquifer will not be a linear function of its storage (Potter and Gburek, 1986). For example, the change in water level for an aquifer with a triangular longitudinal section will be a decreasing function of its de-watered volume, and discharge will be weakly non-linear as the aquifer drains (Konrad, 2006a).

Hydrograph Separation

Separation of streamflow into baseflow and surface-flow components is a long-standing but fundamentally “arbitrary” practice in hydrology (Linsley and others, 1982) because baseflow and surface flow are concepts rather than distinct

physical entities. Baseflow is a part of the conceptual basis of many process-based land-surface hydrology models. It is used to estimate groundwater recharge and streamflow during periods without rainfall or snowmelt.

Algorithms for hydrograph separation rely on both heuristics and empiricism—they depend on defined periods when streamflow is primarily baseflow and rules for interpolating baseflow between these periods (Nathan and McMahon, 1990; Sloto and Crouse, 1996; Rutledge, 1998). Where streamflow has different sources (for example, precipitation and groundwater), hydrographs can be separated using the ionic or isotopic signatures of the source water in a mixing model (Stewart and others, 2007; Miller and others, 2014). Conceptually, chemical hydrograph separation distinguishes baseflow as water that resided in soil and aquifers long enough to acquire a distinct chemical signature rather than the response time of streamflow to precipitation or snowmelt and, thus, are not equivalent to other separation methods (Raffensperger and others, 2017a). Hydrographs can be separated into additional components to distinguish streamflow variability at different time scales (for example, interflow) for more refined differentiation of sources (Curtis and others, 2020).

BFS has a state-space structure, where baseflow is a function of water stored in a base reservoir (an unmeasured state variable), which gives BFS capability to predict baseflow during dry periods. BFS uses a non-linear function to relate baseflow discharge to base-reservoir storage to improve its performance over long-time scale (weeks to months) in comparison to a linear-reservoir model that presumes streamflow is a linear function of storage. The nonlinear model presumes that the first-order recession rate, $(dQ/dt)/Q$, decreases over time such that baseflow approaches a relatively steady value, so it is not appropriate for situations where streams dry up rapidly.

The state-space structure with unmeasured storage variables distinguishes BFS from graphical hydrograph separation models (Nathan and McMahon, 1990; Rutledge, 1998). In contrast to graphical hydrograph separation, the state-space structure imposes hydraulic constraints on the baseflow component of streamflow through the discharge-storage relation for the base reservoir that is based on Darcy's law and conservation of mass for infiltration, recharge, storage, and streamflow components flow. The storage terms in the space-state structure of BFS give it the capability to forecast streamflow during dry periods when streamflow is generated by drainage of water stored in a stream basin. In this case, BFS must be calibrated so that baseflow represents reliably available streamflow over time.

Baseflow as the relatively steady component of streamflow is a standard conception (Linsley and others, 1982) but differs from chemical hydrograph separation, which defines baseflow as water that has resided in soil matrix or aquifers and has acquired a distinct geochemical signature measurable through dissolved solutes or decay of isotopes when compared to precipitation or surface runoff (Stewart and

McDonnell, 1991; Stewart and others, 2007). Nonetheless, the state-space structure of BFS provides the capability to calculate groundwater residence times, which could be used to advance chemical-based hydrograph separation that relies on end-member mixing models (Miller and others, 2014; Raffensperger and others, 2017a) by allowing the chemistry of groundwater and, thus baseflow, to evolve over time.

Model Description

BFS is a spatially aggregated, two-reservoir model to simulate streamflow recession over times scales of days to months (Konrad, 2020). BFS has a state-space structure (Durbin and Koopman, 2012) with non-linear functions to represent storage-discharge relations for the reservoirs. Impulses representing rainfall or snowmelt are generated endogenously (Kirchner, 2009) by BFS for time steps when streamflow increases, so streamflow and the drainage area of the stream are the only data required to calibrate and run BFS. The model tracks reservoir storage and conserves mass over time allowing the calculation of residence time in the basin. Once storage is initialized, a calibrated model can be used to forecast streamflow during dry periods.

Streamflow is conceptualized as the sum of three components: baseflow, $Q_b(t)$, surface flow, $Q_s(t)$, and direct runoff, $Q_d(t)$:

$$Q(t) = Q_b(t) + Q_s(t) + Q_d(t). \quad (2)$$

Baseflow represents the relatively steady component of streamflow generated from groundwater discharge through longer and deeper subsurface flow paths, drainage from lakes, meltwater from glaciers and snowfields, and gradually varied flow through river channels and their corridors (hyporheia and floodplains). Surface flow represents runoff through short and shallow flow paths that connect surface storage to the stream network such as lateral flow through soil and drainage from surface depressions, but also includes snowmelt and flood water routing quickly through stream networks. Direct runoff represents runoff of precipitation and snowmelt from saturated or other impervious surfaces connected to the stream network.

BFS calculates impulses of water, which generates direct runoff and infiltrates into the surface reservoir. Water stored in the surface reservoir recharges the base reservoir and generates surface-flow component of streamflow. Discharge from the base reservoir generates the baseflow component of streamflow. In addition to the six fluxes (impulses, infiltration into the surface reservoir, recharge into the base reservoir, direct runoff, surface discharge, and base discharge), BFS simulates storage in the surface reservoir and in the base reservoir. The saturated thickness of each reservoir and the spatial extent of land surface and channel saturation are determined from reservoir storage and geometry.

Conceptual Stream Basin and Flow System

BFS represents a stream basin as rectangular dihedral (shaped like an “open book”) where two symmetrical hillslopes are drained along their shared edge at the center of the dihedral by a stream channel (fig. 1). The basin has a length of L_b and width of W_b . Hillslopes form the surface reservoir providing depression and soil storage for precipitation and snowmelt, conveying rapid-response runoff to the channel, and recharging the underlying, unconfined aquifer that comprises the base reservoir. The base reservoir has the same length and width as the basin (L_b and W_b) and a thickness that varies as a function of distance from its downstream end but is uniform for any cross section of the basin. The surface reservoir has a width (oriented perpendicular to surface flow, parallel to baseflow) that is equal to the basin length, L_b . The saturated depth of the surface reservoir at a point in time, $Z_s(t)$, determines surface flow and the spatial extent of the land-surface saturation. Impulses of precipitation/snowmelt, $I(t)$, generate direct runoff from the saturated portion of the land surface while infiltration, $F(t)$ of those impulses is only permitted through the unsaturated portion of the land surface (table 1). The saturated depth of the base reservoir, $Z_b(t)$, determines baseflow and the saturated

length of stream channel, and the area for recharge. L_b , W_b , $Z_s(t)$, and $Z_b(t)$ are “hydraulically effective” variables for a site not basin morphometrics that can be measured.

BFS can be applied to basins that do not fit the conceptual system provided they can be distilled into two reservoirs with stable storage-discharge relations. The model does not explicitly represent regional groundwater fluxes into or out of the stream basin. It can be applied to streams where snowmelt generates surface flow and recharges the base reservoir.

The lower boundaries of both reservoirs and flow in the reservoirs are assumed to be horizontal. Flow in the surface reservoir is lateral (perpendicular) to the stream channel and governed by the cross sections at $X_s(t)$ on both sides of the channel where the water surface intersects the land surface. Flow in the base reservoir is longitudinal (parallel) to the stream channel and governed by the cross section at $X_b(t)$ where the water surface in the base reservoir intersects the channel. The water-surface elevation is horizontal from $X_b(t)$ to L_b . The stream channel acts as a perfectly efficient drain for all water in the base reservoir above the channel elevation at any cross section of the valley. Lateral flow in the base reservoir is presumed to be subordinate to longitudinal flow and a response to local hydraulic gradients resulting from seepage into the channel that do not control the overall rate of aquifer discharge (Konrad, 2006b).

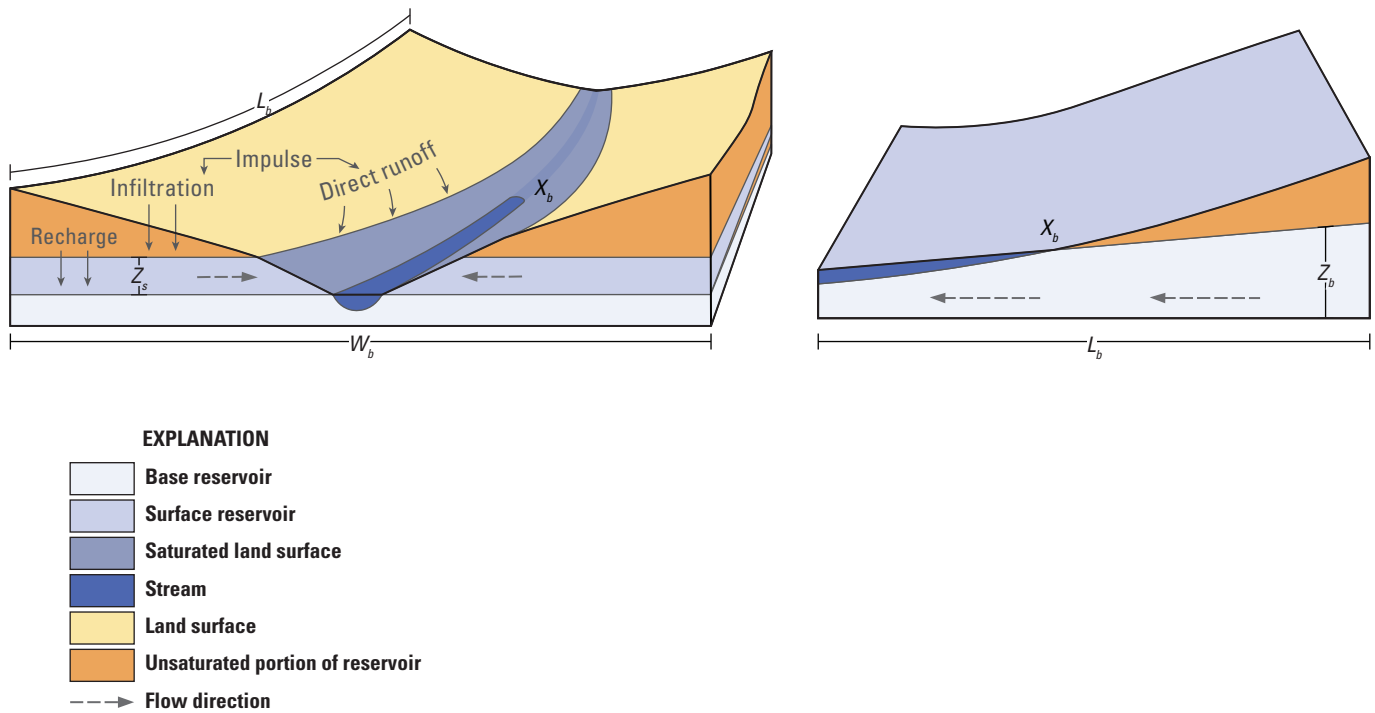


Figure 1. Oblique view of the conceptual stream basin (left image) with a longitudinal section of the surface reservoir showing its saturated thickness, Z_{sr} , at the point where the water surface intersects the land surface and longitudinal section of the base reservoir (right image) with its saturated thickness, Z_b , at the point where its water surface intersects the channel, X_b . L_b , basin length; W_b , basin width.

Table 1. Flux calculations.

[For definitions of equation variables, see the corresponding report equation]

Flux	Description	Equation	Corresponding report equation number
Impulse (I)	Water added in a time step when streamflow increases to minimize error for the time step	$I(t^*) = 2 \frac{\epsilon(t^*)}{W_b X_s(t^*)}$ where t^* is limited to time steps when streamflow increases or the first time steps of recession periods	13
Infiltration (F)	Portion of the impulse that enters the surface reservoir	$F(t) = 2 X_b(t) \left[\frac{W_b}{2} - \frac{Z_s(t)}{\alpha} \right] \min[K_z, I(t)]$	14
Surface discharge (Q_s)	Flow out of surface reservoir into stream	$Q_s(t) = 2 L_b K_s \alpha Z_s(t)$	9
Direct runoff (Q_d)	Product of impulse depth and saturated land surface	$Q_d(t^*) = 2 I(t^*) W_b X_s(t^*)$	15
Recharge (R)	Portion of surface storage that flows into base storage	$R(t) = [L_b - X_b(t)] W_b \min[K_z, POR Z_s(t)]$	16
Base discharge (Q_b)	Flow out of base reservoir into stream	$Q_b(t) = W_b K_b Z_b(t) \frac{dZ_b}{dx}$	8

Relation of Surface-Reservoir Storage to Saturated Thickness

Storage in each reservoir is a non-linear function of the saturated thickness of the reservoir. As a result, discharge from each reservoir is first-order non-linear—the fraction change in streamflow over time, $(dQ/dt)/Q$, is not constant. The surface reservoir is presumed to have a triangular longitudinal section where the upper boundary has a slope, α , and the lower boundary is level with the channel. To maintain this geometry along the length of the channel, the upper and lower boundaries of the surface reservoir would have longitudinal gradients (parallel to the channel), β , equal to the channel gradient. Longitudinal flow in the surface reservoir, however, is assumed to be negligible, which requires that $\alpha > \beta$. The saturated thickness of the surface reservoir, Z_s , is specified as a linear function of lateral distance from the channel, X_s (fig. 2A):

$$Z_s(X_s) = \alpha X_s, \quad (3)$$

using the utility function sur_z (table 2). The hydraulic gradient for discharge from the surface reservoir is equal to α (Konrad, 2006a). With these specifications, discharge from the surface reservoir is only weakly non-linear— $(dQ/dt)/Q$ approaches a constant value as the surface reservoir drains (fig. 2C).

Relations of Base-Reservoir Storage and Saturated Thickness

The relation between storage in the surface reservoir, S_s , and its saturated thickness, Z_s , can be derived from its geometry as

$$S_s(t) = X_b(t) Z_s(t) POR (W_b(t)/4 + Z_s(t)/2\alpha), \quad (4)$$

where

POR is the drainable porosity.

Storage in surface reservoir is calculated using the utility function sur_store (table 2). The base reservoir has a thickness, $Z_b(t)$, that is specified as a power function of longitudinal distance from the basin outlet, x :

$$Z_b(t) = \left[\frac{X_b(t)}{X_1} \right]^\beta, \quad (5)$$

where

X_1 and β are parameters that affect the thickness and shape of the upper surface of the base reservoir.

6 **BFS—A Non-Linear, State-Space Model for Baseflow Separation and Prediction**

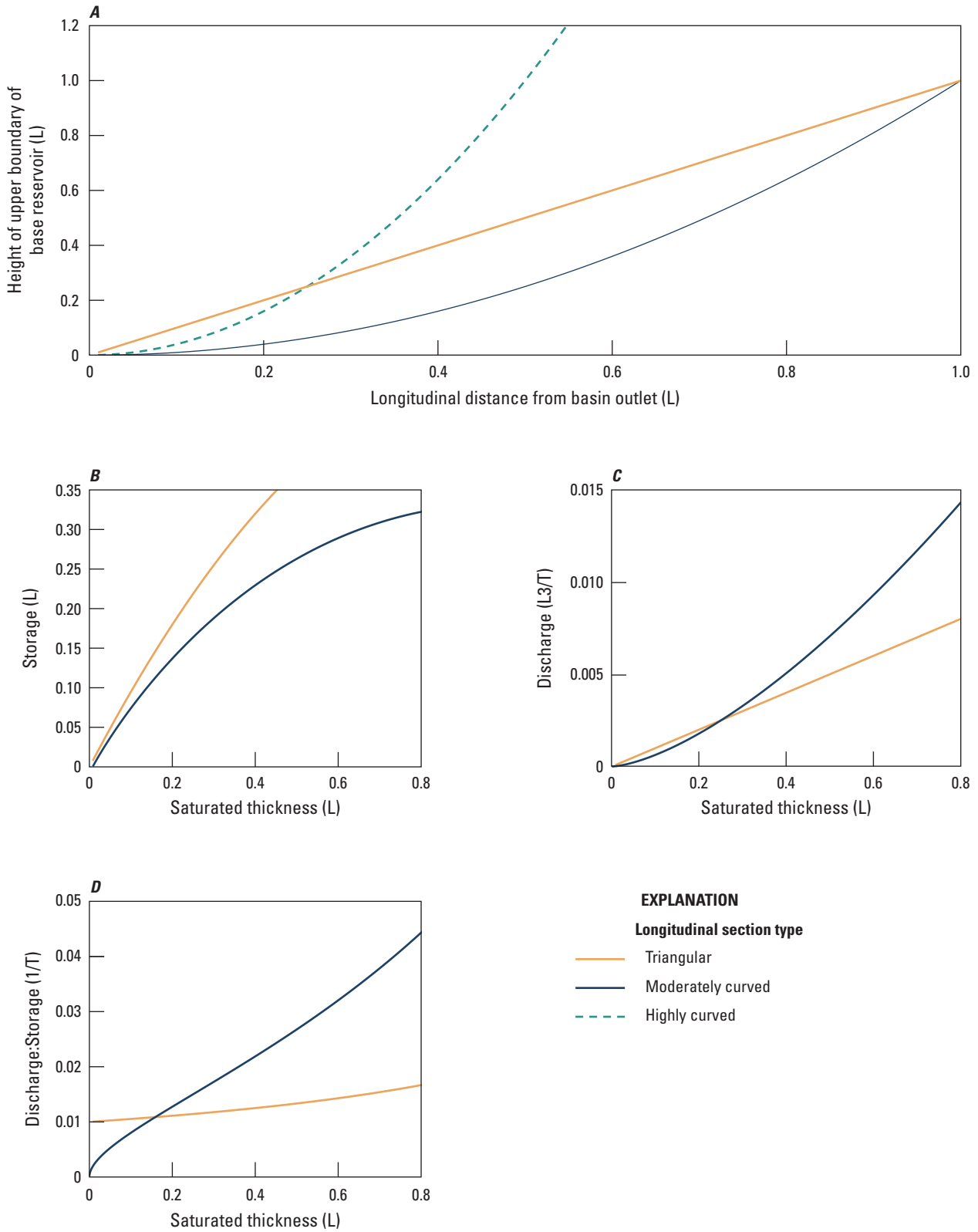


Figure 2. Examples of longitudinal sections of reservoirs (A) with parameters for equation 4—a reservoir with a triangular longitudinal section ($X_1 = 1, \beta = 1$); moderately curved longitudinal section ($X_1 = 1, \beta = 2$); and highly curved longitudinal section ($X_1 = 0.5, \beta = 2$). Storage (B), discharge (C), and ratio of discharge to storage for the triangular and moderately curved longitudinal sections using additional parameters $L_b = 1, W_b = 1, K_b = 1,$ and $POR = 1$. The discharge-to-storage ratio (D) is constant with storage for linear first-order recession (not shown).

Table 2. Description of functions used for the baseflow separation model.

Function	Arguments	Description
<i>bf_sep</i>	<i>qin, timestep, error_basis, basin_char, gw_hyd, flow</i>	Main function to calculate storage and fluxes, generates impulses, averages the initial and final estimates of fluxes for each time step for the water balance, calculates errors, and writes output to file; function returns the mean weighted absolute percent error to support calibration using the R function <i>optim</i> .
Utility functions		
<i>base_table</i>	$L_b, X_b, \beta, W_b, K_b, POR$	Creates a table with Z_b , hydraulic gradient (dZ_b/dx), S_b , and Q_b for 1,202 values of X_b from 0 to L_b .
<i>sur_z</i>	$\alpha, W_b/2, POR, S_s$	Calculates the saturated thickness of the surface reservoir, Z_s , given the parameters for equation 4 and the volume of water stored in the surface reservoir, S_s .
<i>sur_store</i>	$\alpha, W_b/2, POR, Z_s$	Calculates S_s given the parameters for equation 4 and Z_s (inverse of <i>sur_z</i>).
<i>sur_q</i>	L_b, α, K_s, Z_s	Calculates discharge from the surface reservoir, Q_s , given the parameters for equation 11 and Z_s .
<i>dir_q</i>	L_b, α, Z_s, I	Calculates direct runoff, Q_d , given an impulse, I , and the saturated thickness of the surface reservoir, Z_s .
<i>infiltration</i>	$L_b, W_b/2, K_s, \alpha, Z_s, I$	Calculates infiltration, F , of a portion of the impulse into the surface reservoir.
<i>recharge</i>	$L_b, X_b, W_b/2, K_s, Z_s, POR$	Calculates recharge, R , from the surface reservoir into the base reservoir.
<i>bf_ci</i>	<i>bf_mod_out</i>	Creates an array with confidence intervals for simulated streamflow.
<i>flow_metrics</i>	$Q_{in}, timestep$	Creates a six-element vector with flow metrics used in <i>bf_sep</i> .

The exponent β controls the curvature of the base reservoir's upper surface and, as a result, the nonlinearity of discharge as a function of storage (fig. 2). The coefficient $X1$ adjusts the saturated thickness of the base reservoir relative to its length. Flow under the stream channel at the site ($X=0$) is ignored. The saturated thickness of the base reservoir is calculated using the utility functions *base_table*.

Equation 5 allows limited independence of the base reservoir's saturated thickness, $Z_b(t)$, from its hydraulic gradient, dZ_b/dx , but both increase with distance from the basin outlet. The hydraulic gradient at the point where its water surface intersects the channel, $X_b(t)$, governs discharge from the base reservoir and is equal to the slope of upper boundary of the base reservoir,

$$\frac{dZ_b}{dx} = \beta \frac{X_b(t)^{\beta-1}}{X_1^\beta}. \quad (6)$$

Reservoirs with triangular or concave upper surface, $\beta \leq 1$, will drain at a rate that approaches first-order linear (fig. 2C) as the dewatered volume of reservoir become proportional to the dewatered thickness of the reservoir. When $\beta > 1$, the base reservoir has a concave upper boundary and will drain rapidly when it fully saturated. As the reservoir drains, the first-order recession rate, $(dQ/dt)/Q$, decreases and can approach zero (steady baseflow).

Calculating storage in the base reservoir directly from equation 5 requires integration of a non-linear equation. Alternatively, storage in the base reservoir can be approximated each time step given the location where the water surface in the base reservoir intersects the stream

channel, $X_b(t)$, by summing the water stored in closely spaced vertical sections that have a length of Δx from $x = 0$ to $X_b(t)$ and the water in the reservoir from $X_b(t)$ to L_b :

$$S_b(t) = POR W_b \left[\frac{\sum_{x=0}^{X_b(t)} Z_b(x) \Delta x}{+ Z_b(X_b(t)) (L_b - X_b(t))} \right], \quad (7)$$

with a drainable porosity of POR , a water surface height $Z_b(x)$ given by equation 5, and a width of W_b . The first term in equation 7, $\sum_{x=0}^{X_b(t)} Z_b(x) \Delta x$, represents water stored between $x = 0$ and $x = X_b(t)$ where the base reservoir is saturated to its upper surface and the second term, $Z_b(X_b(t))(L_b - X_b(t))$, represents water stored from $x = X_b(t)$ to L_b (fig. 1), where the saturated thickness is $Z_b(X_b(t))$. This numerical approach for calculating $S_b(t)$ as a function of $X_b(t)$ (eq. 7) is implemented via the utility function *base_table*.

Storage-Discharge Relations for Surface and Base Reservoirs

Discharge from the surface and base reservoirs, $Q_s(t)$ and $Q_b(t)$, respectively, is conceptualized as saturated flow through a porous medium and quantified using Darcy's law applied at the cross section where the reservoir's water surface intersects the reservoir's upper boundary where storage-discharge relations for the reservoirs are specified using their water levels. Discharge from the base reservoir is calculated using Darcy's law at $X_b(t)$,

$$Q_b(t) = W_b K_b Z_b(t) \frac{dZ_b}{dx}, \quad (8)$$

where

- K_b is hydraulic conductivity for the base reservoirs,
- W_b is the width of the base reservoir,
- $Z_b(t)$ is the saturated thicknesses of the base reservoir at the section where the base water surfaces intersect the channel, and
- dZ_b/dx is estimated from [equation 5](#) for $x = X_b(t)$.

Discharge from the surface reservoir is

$$Q_s(t) = 2L_b K_s \alpha Z_s(t), \quad (9)$$

where

- K_s is hydraulic conductivity for the surface reservoir,
- L_b is the width (perpendicular to flow) of surface reservoir, and
- $Z_s(t)$ is saturated thicknesses of the surface reservoir at the section where the water surface intersects the land surface.

Water Balance

BFS uses a water balance to calculate storage in the base reservoir, S_b , and in the surface reservoir, S_s , which are updated each time step based on:

$$S_b(t+1) = S_b(t) - Q_b(t) + R(t), \quad (10)$$

$$S_s(t+1) = S_s(t) - Q_s(t) + F(t) - R(t), \quad (11)$$

where

- $R(t)$ is recharge of the base reservoir from the surface reservoir and
- $F(t)$ is infiltration of rainfall or snowmelt into the surface reservoir.

A second-order Runge-Kutta approach (Clark and Kavetski, 2010) is used to calculate the water balance—the fluxes ($Q_b(t)$, $Q_s(t)$, $R(t)$, and $F(t)$) in [equations 10](#) and [11](#) are estimated for the beginning and the end of the time step and averaged. Initial estimates of the fluxes are calculated from [equations 3](#) and [5](#) using the saturated thickness for each reservoir from the previous time step. Storage for the reservoirs are updated using the initial values of the fluxes in [equations 10](#) and [11](#). The fluxes are re-calculated for the updated storage values and averaged with their initial value for the time step to calculate the final value of storage in [equations 10](#) and [11](#) for the time step. Errors from this numerical approximation may be large during periods of high flow when storage is changing rapidly, but generally are negligible during dry periods.

Impulses, Direct Runoff, Infiltration, and Recharge

To maintain the water balance, BFS generates impulses of water to the land surface representing rain and snowmelt. Impulses produce direct runoff from saturated land surfaces, Q_d , and infiltration, F , through unsaturated land surfaces into the surface reservoir ([fig. 1](#)). In the framework of state-space modeling, impulses are used to update surface storage to minimize model error. As a result, errors for time steps with impulses do not indicate the predictive performance of BFS and are excluded when calculating model error for a simulation.

Impulses are generated in time steps when streamflow increases more than a specified fraction (*Frac4Rise*, [table 3](#)). The value of *Frac4Rise* should be set to filter out high frequency measurement error and fluctuations in streamflow not related precipitation or snowmelt, which can be large in shallow or tidal streams. Impulses are allowed in the time step immediately after an increase in streamflow to account for decreasing rates of rainfall or snowmelt at the end of a direct runoff event. Otherwise, impulses are not generated in time steps when streamflow has recessed longer than 1 day.

The impulse algorithm starts by calculating the magnitude of the impulse needed so that direct runoff from saturated surfaces, $Q_d(t^*)$, will account for the residual, ϵ , between measured streamflow and the sum of surface flow and baseflow for a time step with an impulse, t^* ,

$$\epsilon(t^*) = Q(t^*) - Q_b(t^*) - Q_s(t^*). \quad (12)$$

The impulse needed to generate $Q_d(t^*)$ from saturated land-surface areas during t^* is calculated:

$$I(t^*) = 2 \frac{\epsilon(t^*)}{W_b X_s(t^*)}. \quad (13)$$

The impulse is then applied to the unsaturated area of the land surface to calculate $F(t^*)$,

$$F(t^*) = 2 X_b(t^*) \left[\frac{W_b}{2} - \frac{Z_s(t^*)}{\alpha} \right] \min[K_2, I(t^*)]. \quad (14)$$

Surface storage and $X_s(t^*)$ are updated to account for infiltration. Direct runoff is re-calculated to account for the expansion of the saturated area as:

$$Q_d'(t^*) = 2 I(t^*) W_b X_s(t^*). \quad (15)$$

The updated value for direct runoff will exceed time-step error, $Q_d'(t^*) > \epsilon(t^*)$ because of the expansion of saturated surfaces in response to infiltration of the impulse. The algorithm reduces $I(t^*)$ incrementally, recalculates $F(t^*)$, $S_s(t^*)$, $Z_s(t^*)$, $X_s(t^*)$, and $Q_s(t^*)$ until $Q_d'(t^*) \sim \epsilon(t^*)$ within a tolerance of the larger of 0.01 $Q(t^*)$ or low-flow measurement precision, *Prec*.

Table 3. Parameters describing streamflow characteristics in the vector *flow* used as an argument in the function *bf_sep*.

[/, divided by]

Parameter	Description	Dimensions	Role of parameter
Q_{thresh}	Threshold (minimum) streamflow that is greater than measurement precision and above which the absolute value of first-order recession rates, $ \Delta Q/Q $, increase with streamflow.	Volume/Time	Initialization of baseflow; calculation of model error for time steps when measured streamflow is greater than the threshold.
R_s	First-order coefficient for surface flow recession. R_s has a negative value. The 95th percentile of 2-day recession rates (a relatively slow rate) is used for initial calibration (eq. 17).	1/Time	Forces initial calibration of surface reservoir parameters so surface reservoirs supports recession rates up to R_s , does not constrain final calibration.
R_{b1}	First-order coefficient for rapid baseflow recession. R_{b1} has a negative value. The 50th percentile of 10-day recession rates, typical rate) is use for initial calibration (eq. 18).	1/Time	Forces initial calibration of base reservoir parameters so base reservoir supports recession rates up to R_{b1} , does not constrain final calibration; used for weighting time-step errors when <i>error_basis</i> ='total'.
R_{b2}	First-order coefficient for rapid baseflow recession. R_{b2} has a negative value. The 95th percentile of 10-day recession rates (a relatively slow rate) is use for initial calibration (eq. 18).	1/Time	Forces initial calibration of base reservoir parameters so base reservoir supports recession rates of at least R_{b2} , does not constrain final calibration; used for weighting time-step errors when <i>error_basis</i> ='base'.
<i>Prec</i>	Precision of low-flow values based on the difference between the 0.01 quantile of streamflow and the next lower reported value.	Volume	Precision is used to classify recessional time steps and to calculate percentage of error for calibration.
<i>Frac4Rise</i>	Fractional change to identify a rise in streamflow (0.05).	Dimensionless	Impulses are calculated for time steps when streamflow increases by at least <i>Frac4Rise</i> .

Recharge links storage in the two reservoirs and is calculated using as the product of the unsaturated area of the base reservoir, $(L_b - X_b(t)) W_b$, and the smaller of either the vertical hydraulic conductivity, K_z , or the depth of water in the surface reservoir, Z_s :

$$R(t) = \frac{[L_b - X_b(t)] W_b \min[K_z, n Z_s(t)]}{n} \quad (16)$$

The factor $L_b - X_b$ limits recharge to the unsaturated portion of the base reservoir (upstream from X_b), which in turn can act to limit the maximum rate of baseflow.

Model Implementation

BFS is implemented with a set of functions (table 2) in the statistical programming language R (R Core Team 2020a). The main function, *bf_sep*, calls on utility functions for storage and flux calculations, generates impulses, averages the fluxes for each time step, calculates errors, and writes a file with the simulation results.

The function *bf_sep* has six arguments—a numerical vector, Q_{in} , with the time series of measured streamflow volume for each time step (missing values indicated by

NA); a character string, *timestep*, that has a value of either “daily” or “hourly” indicating the time step; a character string, *error_basis*, that has a value of either “base” or “total” indicating which simulated streamflow components are used for error calculations; a six-element numeric vector, *flow*, with parameters characterizing streamflow; a five-element vector, *basin_char*, with parameters characterizing the geometry of stream basin and reservoirs; and a five-element vector, *gw_hyd*, with hydraulic parameters. Streamflow must be entered as a volume [L³] for each time step with the same units of length as parameters.

Model Parameters

BFS requires 16 parameters entered as 3 vector arguments to the function *bf_sep* (tables 2, 3, and 4). Eight parameters can be assigned values as described in this section; the remaining eight parameters must be calibrated. Nine utility functions (table 2) are called by *bf_sep* for model calculations. These functions retrieve parameter values from the environment where *bf_sep* was called. All parameters must have positive values except for the three recession rate constants (R_s , R_{b1} , and R_{b2} ; table 3), which must have negative values. The time units for the parameters must be consistent with the time step (daily or hourly) and the length units for

Table 4. Parameters defining the geometry of the stream basin in the vector *basin_char* used as an argument to the function *bf_sep*.

Parameter	Description	Dimensions	Use of parameter
<i>Area</i>	Measured (surface) drainage area upstream from the site	Area	Conversion of depths and volumes, limits the product of basin length (L_b) and width (W_b)
L_b	Effective length of stream basin and channel, width of base reservoir	Length	Factor for base and surface storage and recharge
X_1	Scaling parameter for base reservoir thickness as a function (eq. 5)	Length	Base storage-discharge function
W_b	Effective base reservoir width	Length	Base storage-discharge function, recharge, surface storage
<i>POR</i>	Effective drainable porosity	Dimensionless	Relations for storage (base and surface) as a function of saturated thickness

the parameters must be consistent with the length unit of streamflow volume (table 3). The elevation of the upper surface of base reservoir and discharge from the base reservoir must be defined over the interval from $X_b = 0$ to L_b as positive and finite. If any of these conditions are not met or if $L_b \times W_b > Area$, *bf_sep* will return an error.

The vector, *flow*, (table 3) has six parameters used to initialize baseflow, to identify time steps when impulses will be calculated, and for calibration of other parameters. The parameters in *flow* are not calibrated—a user can adjust these at their discretion to change how baseflow and surface flow are defined. Alternatively, the function *flow_metrics* can be used to generate these parameters (table 2) from the time series of streamflow at a site. Three of the parameters in *flow* are used in the main function, *bf_sep*: the minimum threshold, Q_{thresh} , for error calculations; the precision, *Prec*, of low-flow measurements; and the fractional increase, *Frac4Rise*, used to distinguish high-frequency noise in streamflow measurements from an increase in streamflow resulting from precipitation, snowmelt, or reservoir releases. Model errors are not used for time steps when $Q(t) < Q_{thresh}$. Q_{thresh} should be set to the larger of the minimum, non-zero streamflow or the streamflow with the lowest, non-zero first-order recession rate, $[Q(t) - Q(t+1)]/Q(t)$. When $Q_{in} < Q_{thresh}$, first-order streamflow recession rates increase as streamflow decreases (for example as a stream dries up). First-order recession rates that increase as streamflow decreases are not represented by equations 5 and 8, so baseflow simulations during these time steps are not reliable. Measurement precision for low flows, *Prec*, can be set by using the difference between the two lowest streamflow values in a record. *Prec* is used as the tolerance for small errors in simulated streamflow and allows fractional errors to be calculated when $Q(t) = 0$. The fractional increase in streamflow, *Frac4Rise*, must be specified to identify time steps with an impulse. A nominal value of *Frac4Rise* = 0.05 can be used so that measurement error or small fluctuations in streamflow do not trigger an impulse.

The other three parameters, R_s , R_{b1} , and R_{b2} , in the *flow* are first-order recession rates for different time scales of hydrologic response. Although these three parameters do

not affect calculations in *bf_sep*, values must be included in the vector used as the argument *flow* for *bf_sep* to facilitate initialization of parameter during calibration. Because of nonlinear streamflow recession, first-order recession rates are not constant and typically decrease for longer time scales (Konrad, 2006a). The utility function *flow_metrics* assigns the first-order recession coefficient for surface flow, R_s , as the 95th percentile of the distribution of all 2-day recession rates:

$$R_s = \ln(Q(t+2)/Q(t))/2, \quad (17)$$

where

t is any time step when $Q(t) > Q_{thresh}$ and $Q(t) > Q(t+2)$, and the daily change in streamflow is less than *Frac4Rise* on days $t+1$ and $t+2$.

The two first-order recession coefficients for baseflow, R_{b1} and R_{b2} , are assigned by *flow_metrics* using the distribution of 10-day recession rates:

$$R_b = \ln(Q(t+10)/Q(t))/10, \quad (18)$$

where

t is any time step when $Q(t) > Q_{thresh}$, $Q(t) < Q_{mean}$, $Q(t) > Q(t+10)$, and the daily change in streamflow is less than *Frac4Rise* for days $t+1$ through days $t+10$.

The typical baseflow recession rate, R_{b1} , is assigned the median value of R_b . The slower recession rate at long-time scales (after an extended dry period), R_{b2} , is assigned the 95th percentile of R_b (slow recession rates are represented by higher percentile because $R_b < 0$).

The vector, *basin_char*, has five parameters defining the effective geometry of the stream basin (table 4). The area of the basin, *Area*, is the measured drainage area upstream from the site. The effective basin length, L_b , is oriented in the direction of the channel and the effective width, W_b , is perpendicular to the channel. Because flow in the surface reservoir is perpendicular to flow in the base reservoir, the width of the surface reservoir is equal to the basin length, L_b .

The function, *bf_sep*, will return an error if $L_b \times W_b > Area$. The scaling parameter for the base reservoir, X_1 , affects the thickness and hydraulic gradient of the base reservoir (eqs. 4 and 5). The parameter, *POR*, is the effective drainable porosity, which affects the relation between storage and saturated thickness of the base and surface reservoirs.

The vector, *gw_hyd*, has five parameters used to calculate the fluxes into and out of the reservoirs and relations between storage in and discharge from each reservoir (table 5). These parameters include the hydraulic gradient of the surface reservoir, α ; the exponent for the upper boundary of the base reservoir, β in equation 3, which determines the hydraulic gradient of the base reservoir (eq. 5); the horizontal and vertical hydraulic conductivities of the surface reservoir, K_s and K_z , respectively; and the horizontal hydraulic conductivity of the base reservoir, K_b .

Order of Calculations

BFS calculates the two storage variables, $S_b(t)$ and $S_s(t)$, and the six flux variables, $I(t)$, $Q_d(t)$, $F(t)$, $Q_s(t)$, $R(t)$, and $Q_b(t)$, for each time step t . Fluxes at the beginning of the time step are estimated based on storage for the previous time step ($t-1$), which provides values of $Z_b(t)$ and $Z_s(t)$ for the time step via equations 3 and 5. The initial flux estimates are used in the water balance (eqs. 10 and 11) to make preliminary estimates of storage for time step t . The fluxes are recalculated using the preliminary estimates of the storage for time step t and averaged with their initial estimates. Equations 10 and 11 are updated using the mean values of the fluxes to calculate storage for the time step.

During a simulation, storage and fluxes must have finite, real, and positive values. Discharge from the reservoirs is limited to storage at the beginning of the time step plus any inflow (infiltration for the surface reservoir and recharge for the base reservoir). Infiltration and recharge are limited to the sum of available storage and discharge from the receiving reservoir.

The function *bf_sep* assigns values to individual parameters from the input vectors *basin_char* (lines 21–26), *gw_hyd* (lines 32–36), and *flow* (lines 42–48). It calls the utility function *base_table* to create a table that has base storage (S_b), base discharge (Q_b), thickness (Z_b), and the water surface gradient (dz/dx) at X_b , where the base water surface intersects the stream, for a series of discrete values of X_b from 0 to L_b . Using pre-calculated values of base reservoir variable increases the efficiency of the model compared to calculating the base variables in each time step. The table is limited to 1,202 values of X_b to balance the efficiency and resolution of using pre-calculated values for S_b , Q_b , and dz/dx : increasing the number of values of X_b will increase resolution of the variables but increase the time required to run the model. To limit errors from using the discrete rather than continuous values of S_b , Q_b , Z_b , and dz/dx , the first 101 values of X_b span the range corresponding to $Q_b = 0$ to Q_{thresh} , the next 1,000 values of X_b span the range corresponding $Q_b = Q_{thresh}$ to Q_{mean} , and the last 101 values of X_b span the range corresponding from $Q_b = Q_{mean}$ to the maximum possible value of Q_b at $X_b = L_b$. The discrete values of base reservoir storage and discharge reduces the precision of baseflow when $Q_b < Q_{thresh}$ and $Q_b > Q_{mean}$ such that Q_b can appear to be stepped rather than smoothly varying in a hydrograph.

Table 5. Hydraulic parameters in the vector *gw_hyd* used as an argument to the function *bf_sep*.

[/, divided by]

Parameter	Description	Dimensions	Use of parameter
α	Effective lateral hydraulic gradient of surface reservoir	Dimensionless	Determines the depth and slope (hydraulic gradient) of upper surface of surface reservoir as a function of distance to channel
β	Exponent for base water surface function	Dimensionless	Determines the depth and slope (hydraulic gradient) of upper surface of base reservoir as a function of distance from basin outlet
K_s	Effective hydraulic conductivity of surface reservoir	Length/Time	Infiltration into and discharge from surface reservoir
K_b	Effective horizontal hydraulic conductivity of base reservoir	Length/Time	Discharge from base reservoir
K_z	Effective vertical hydraulic conductivity of base reservoir	Length/Time	Recharge from surface reservoir into base reservoir

Initial Conditions

Surface and base storage are specified for the initial time step (*bf_sep*, lines 115–127), assuming baseflow is equal to the threshold streamflow: $Q_b(1) = Q_{thresh}$. The initial surface flow is the difference between measured streamflow and the initial baseflow, $Q_s(1) = Q(1) - Q_b(1)$. Surface storage is then determined from $Q_s(1)$ using (2) and (3). Base storage is determined from $Q_b(1)$ using (4) and (5). Simulated baseflow will be influenced by the initial storage value until there have been a series of impulse and the base reservoir is recharged. The first 100 days (or 2,400 hours) are not included in the calculation of overall model error to limit the effect of initial storage values (lines 242–244).

Estimates at the Beginning of a Time Step

At the beginning of a time step, $X_b(t)$, $Z_b(t)$, $S_b(t)$, $Q_b(t)$, $Z_s(t)$, $S_s(t)$, and $Q_s(t)$ are set equal to their values from the previous time step (*bf_sep*, lines 131–138). Recharge at the beginning of the time step is estimated with the recharge function (table 1) using the saturated thickness of the surface, $Z_s(t-1)$, from the previous time step (*bf_sep*, line 143). Recharge is limited to the storage available in the base reservoir and the initial estimate of baseflow for the time step.

For time steps when $\Delta Q/Q > Frac4Rise$ or the subsequent time step, the impulse algorithm (*bf_sep*, lines 154–169) calculates the impulse depth and direct runoff from saturated surfaces,

$$Q_d(t) = 2 L_b \frac{Z_s(t)}{\alpha} I(t). \quad (19)$$

Surface storage and discharge are assumed to respond instantaneously to the impulse. Surface discharge is updated in the impulse algorithm as,

$$Q_s(t) = X_b \left[Z_s(t-1) + \frac{F(t)}{POR} \right] K_s \alpha. \quad (20)$$

where

$F(t)/POR$ is the rise in the water level in the surface reservoir as a result of infiltration.

The impulse algorithm iteratively reduces the impulse until the streamflow residual is less than 1 percent of measured streamflow or measurement precision: $Q_b(t) + Q_s(t) + Q_d(t) - Q(t) < \max(0.01 Q(t), Prec)$.

Once the impulse has been set, the initial estimate of infiltration into the surface reservoir is calculated using the function infiltration (table 2) as the product of the unsaturated surface area and the smaller of K_z or the impulse (*bf_sep*, line 171). The initial estimate of infiltration is limited to storage available in the surface reservoir at the beginning of the time

step. Any portion of the impulse that cannot be stored, $2 X_b (W_s/2 - Z_s/\alpha) I(t) - F(t)$, is allocated to direct runoff during the time step. For time steps without an impulse, $I(t) = 0$, there is no infiltration, $F(t) = 0$, or direct runoff, $Q_d(t) = 0$.

Estimates at the End of the Time Step

Surface storage is estimated for the end of the time step by adding the initial estimate of infiltration to the initial estimate of surface storage and subtracting the initial estimates of surface flow and recharge (*bf_sep*, line 174). The ending estimate of surface storage is used to estimate saturated thickness of the surface reservoir, surface flow, infiltration, and recharge at the end of the time step (*bf_sep*, lines 175–178). Base storage is estimated for the end of the time step by adding the ending estimate of recharge to initial estimate of base storage and subtracting the initial estimate of baseflow (*bf_sep*, line 179). The ending estimate of base storage is used to estimate the horizontal location where the base water surface intersects the channel, the saturated thickness of the base reservoir, and baseflow at the end of the time step (*bf_sep*, lines 180–182).

The initial and ending estimates flux values are averaged for the time step are averaged and assigned as the final value for the time step (*bf_sep*, lines 186–190). Storage in the surface and base reservoir is calculated using the storage from the previous time step and the mean values of the fluxes for the time step (*bf_sep*, lines 194–206). Direct runoff is updated at the end of the time step to account for the increase in the area of surface saturation during the time step caused by the impulse (*bf_sep*, line 208).

Model Error

The main function, *bf_sep*, returns a mean weighted absolute percent error (“model error”) to the R console to allow calibration using the R function, *optim*, available from stats package (R Core Team, 2020b). The model error returned by *bf_sep* is intended to address three issues particular to model calibration for baseflow separation—(1) the lack of an objective basis for defining baseflow during high flows; (2) the physical constraint that baseflow is always less than or equal to measured streamflow; and (3) the precision of measured streamflow during low flow including high frequency variability (from ice, for example). Without a measure of model performance that addresses these issues, calibration is likely to produce either constant *de minimus* estimates of baseflow that do not represent groundwater dynamics during high flow or dynamic baseflow that underpredicts extremely low flows. Standard performance measures for hydrologic simulation models (Nash-Sutcliffe efficiency, for example) do not explicitly address these issues, but can be calculated from model output.

To facilitate calibration, the argument *error_basis* in *bf_sep* is used to select whether model error will be calculated as the difference between baseflow and measured streamflow (*error_basis* = ‘base’) or as the difference between total flow (sum of baseflow, surface flow, and direct runoff) and measured streamflow (*error_basis* = ‘total’). Model error calculated using *error_basis* = “total” generally will be less than *error_basis* = “base,” which does not include the simulated surface flow or direct runoff components. The ‘base’ option can be used in calibration to maximize the baseflow component. The ‘total’ option can be used as an overall measure of model performance, but calibration using the ‘total’ option can result in relatively steady, *de minimus* baseflow that matches extreme low flows but is otherwise a negligible component of streamflow.

The adjusted percent error in each time step, $\psi(t)$, is calculated in each time step (lines 223 when *error_basis* = ‘base’ or line 225 when *error_basis* = ‘total’) as,

$$\psi(t) = \frac{|Q(t) + Prec - Q_{sim}(t)|}{Q(t) + Prec}, \quad (21)$$

where

$$Q_{sim}(t) \quad \begin{array}{l} Q_s(t) + Q_b(t) \text{ when } error_basis = \text{'total'}, \text{ or} \\ \text{only baseflow, } Q_{sim}(t) = Q(t) \text{ when } error_ \\ basis = \text{'base'}. \end{array}$$

Incorporation of *Prec* in equation 21 reduces the sensitivity of $\psi(t)$ as model residuals approach measurement precision, $Q(t) - Q_{sim}(t) \rightarrow Prec$. Equation 21 also assures that $\psi(t)$ will be finite when *Prec* > 0, which permits application of the model to non-perennial streams.

The adjusted percent error for each time step is assigned a weight, $\omega(t)$, based the inverted baseflow recession curve,

$$\omega(t) = 1 - e^{R_b T(t)} \quad (22)$$

(*bf_sep*, line 227), where

$T(t)$ is the length of recession (time since the last peak in streamflow).

The weight increases from $\omega(t) = 0$ for time steps following a rise in streamflow ($T = 0$) and approaches $\omega(T) = 1$ for extended dry periods ($T \gg 1/R_b$). Two additional conditions are applied to the weights: $\omega(t) = 1$ for any time step when $Q_{sim}(t) > Q(t)$, to penalize simulated baseflow that is greater than measured streamflow (*bf_sep*, line 228); and $\omega(t) = 0$ for any time step when streamflow is less than the threshold, $Q(t) < Q_{thresh}$ (*bf_sep*, line 229), to exclude error for time steps

when streamflow dynamics are not supported by the model. The weight of time steps with direct runoff are set to zero, $\omega(t) = 0$, because direct runoff is calculated to minimize model residual during those time steps.

The overall model error is the mean value of the weighted absolute percent errors starting on day 101 of the simulation (either time step 101 if *bf_sep* argument *timestep* = “day” or time step 2401 if *timestep* = “hour”):

$$\phi = \sum_{t=day}^{end\ day} \psi(t)\omega(t), \quad (23)$$

which is reported directly to the R console by *bf_sep* so that *bf_sep* can be used directly in the function *optim*. The first 100 days of a simulation are censored from the error calculations to reduce the effect of the initial storage values for surface and base reservoirs, but streamflow must increase at some point during the 100-day period to allow infiltration and recharge re-equilibrate storage values. Baseflow should be inspected from the beginning of the simulation and after any gaps in the period of record to assess the effects of initialization of base storage. If baseflow is persistently high or low for longer periods after the start of the simulation and gaps, the rule for assigning initial baseflow can be modified in *bf_sep* (line 115).

Model Output

The function *bf_sep* generates a data frame, *bf_mod_out*, in the active R workspace (table 6), and writes *bf_mod_out* to a comma-delimited text file. Fluxes and storage are reported as volumes [L3] for the time step except for the impulse, which is reported as a depth [L]. The output table includes the length of recession for each time step as the number of time steps since an increase in streamflow, the adjusted percent error, and the weight assigned to the error for the time step.

Model errors do not have a specified analytical distribution that can be used to calculate confidence intervals for streamflow prediction. Instead, model residuals as a fraction of simulated streamflow, $\varepsilon(t) = [Q_{sim}(t) - Q(t)]/Q_{sim}(t)$, are assigned to nine, overlapping bins centered on the 0.1, 0.2, 0.3, ..., 0.9 quantiles of $Q_{sim}(t)$. Each bin spans ± 0.1 of the distribution, for example, the 0.1 bin includes all times steps when $Q_{sim}(t)$ is between the 0 and 0.2 quantiles of all Q_{sim} . Time steps with direct runoff are excluded because direct runoff is calculated to minimize ε . The 0.05 and 0.95 quantiles of ε for each distribution are multiplied by $Q_{sim}(t)$ to calculate the lower and upper confidence bounds for prediction of $Q(t)$.

Table 6. Description of model output, *bf_mod_out*.

Column	Header	Description
1	Date	Date of observation as four digit year, two-digit month, and two-digit day separated by “ - ”
2	Q.L3	Measured streamflow
3	Qpred.L3	Sum of direct runoff, surface flow, and baseflow
4	SurfaceFlow.L3	Discharge from surface reservoir
5	Baseflow.L3	Discharge from base reservoir
6	DirectRunoff.L3	Direct runoff component
7	Eta.L3	Model residual, Q.L3 - Qpred.L3
8	StSur.L3	Surface storage
9	StBase.L3	Base storage
10	Impulse.L	Impulse generated
11	Zs.L	Saturated thickness of surface reservoir where water surface intersects the upper boundary of the base reservoir
12	Zb.L	Saturated thickness of base reservoir where water surface intersects the upper boundary of the base reservoir
13	Infil.L3	Flux from impulse into surface reservoir (infiltration and surface depression storage)
14	Rech.L3	Flux from surface reservoir to base reservoir (recharge)
15	RecessCount.T	The number of consecutive prior time steps since the fractional change in streamflow exceeded <i>Frac4Rise</i> .
16	AdjPctEr	Adjusted percent error: $(Q.L3 + Prec - Baseflow.L3 - SurfaceFlow.L3) / (Q.L3 + Prec \text{ when } error_basis = \text{‘total’}; Q.L3 + Prec - Baseflow.L3) / (Q + Prec \text{ when } error_basis = \text{‘base’})$
17	Weight	Weight for time step error: $1 - \exp(R * RecessCount.T)$ where $R = R_{b1}$ when <i>error_basis</i> = “total”; $R = R_{b2}$ when <i>error_basis</i> = “base”
18	CB0.05	Lower confidence bound for prediction representing the 5 percentile of measured streamflow given predicted streamflow
19	CB0.95	Upper confidence bound for prediction representing the 95th percentile of measured streamflow given predicted streamflow

Model Calibration

BFS was calibrated for low-flow prediction and, secondarily, to maximize the baseflow component of streamflow subject to the constraints of groundwater hydraulics represented by the non-linear relation between base storage and discharge (eqs. 5, 6, and 7) and recharge (eq. 16). Generally, BFS cannot be calibrated so that streamflow will be 100 percent baseflow for all time steps. If simulated baseflow matches measured low flows then it is likely to be much less than measured streamflow during periods of high flow. If simulated baseflow comprises a large fraction of streamflow during periods of high flow, it is likely to exceed measured streamflow during periods of low flow. Calibration, then, must find a balance between parameter sets that allow baseflow to exceed measured streamflow at times and parameter sets that fix baseflow at a relatively constant (*de minimus*) level equal to measured low flows.

Calibration of a state-space baseflow separation model cannot rely on a standard approach of minimizing the error between simulated and measured streamflow without defining periods when streamflow is 100 percent baseflow or using other data (for example, gains in streamflow, the chemical signature of baseflow), indicating the fraction of streamflow comprised by baseflow. Even in these cases, additional constraints on calibration are required or baseflow simulated from a state-space model can exceed measured streamflow at times. In contrast, graphical baseflow separation methods define baseflow as less than streamflow at any point in time (Nathan and McMahon, 1990; Rutledge, 1998). For low-flow simulation, BFS was calibrated by assuming that the baseflow fraction of streamflow increases with time since the last increase in streamflow (length of recession) scaled by R_{b1} (see eq. 19 for the weighting of errors). The weighting of errors implicitly represents the uncertainty of baseflow, which is high when streamflow is high, $Q_b(t) \ll Q(t)$, and low

when streamflow is low, $Q_b(t) \sim Q(t)$. Calibration using errors weighted by recession length will maximize baseflow but is tempered by the full weighting of errors, $\omega(t) = 1$, for time steps when baseflow exceeds streamflow.

The nonlinear function used for the base storage-discharge relation provide a flexible framework that accommodates a wide variety of streamflow regimes but present challenges for calibration (Duan and others, 1992; Kavetski and Kuczera, 2007). Successful calibration of *bf_sep* requires an initial set of parameters that allows a solution of model equations and parameter searches that avoid local minima in the objective. The non-linear relation for base storage and discharge can be highly sensitive to variation in a parameter but only over a limited range of values that depends on other parameter values. As a result, parameter searches must cover a wide range of values at small incremental changes the parameter in the context of combination of other parameters. Thus, calibration may not arrive at the global minimum error or the minimum error may result when baseflow is steady and minimal to avoid exceeding measured streamflow. Although inference on the parameter values is limited, the performance of the resulting model can still be evaluated for low-flow simulation.

A four-step calibration process was developed to provide robust and rapid calibration that maximizes baseflow subject to the constraints of the conceptual model and the penalty for baseflow exceeding measured streamflow for streams from a wide variety of hydro-climatic settings—the conceptual model is constrained to sites where the first-order recession rate of streamflow, $(dQ/dt)/Q$, decreases during dry period; the penalty for time steps when $Q_b(t) > Q(t)$ is full weighting of the error, $\omega(t) = 1$; the model was applied to sites across the US that include arid and humid climates, rain and snow-dominant runoff, and low to high baseflow as a fraction of streamflow. The functions used for calibration are specified

in the file *Rfunctions.bf_calibration.R* and are available in the workspace *Rfunctions.bf_sep_calibration.Rdata* (table 7). The functions are applied in sequence (*cal_initial*, *cal_basetable*, *cal_base*, and *cal_sur*) to find values for eight parameters ($L_b, W_b, X_1, \beta, \alpha, K_s, K_b, K_z$). The other eight parameters (*Area*, *POR*, Q_{thresh} , $R_s, R_{b1}, R_{b2}, Prec, Frac4Rise$) are specified by the user. For this application, *Area* is the measured surface drainage area for the site, *POR* is nominally 0.15, the other parameters are defined in table 2.

Step 1. Initial Calibration with Fixed Parameters for the Base Reservoir

The primary purpose for the initial calibration step is to find a viable set of parameters for running BFS that avoid a *de minimus* baseflow solution. For the initial calibration step, the base reservoir is assumed to have a triangular longitudinal section ($\beta = 1$) and the parameters $L_b, W_b, \alpha, K_s, K_b$, and K_z are optimized for total error, using log scaling of parameters for searching in the *optim* function. The initial calibration using fixed base-reservoir parameters avoids extended searching of non-viable parameter sets, convergence on local minima in model error for simulations with minimal baseflow, and failure to converge on optimal parameters because of off-setting effects from changes in different parameters.

Step 2. Calibration of Storage-Discharge Relation for the Base Reservoir

The second calibration step searches for base-reservoir parameters (X_1, β, K_b, K_z) that permit discharge from the reservoir (baseflow) to have a wide dynamic range with first-order recession rates of R_{b1} when $Q_b = Q_{mean}$ and R_{b2}

Table 7. Calibration functions for baseflow separation model.

Function	Description	Arguments	Parameters to optimize	Minimization Objective
<i>cal_initial</i>	Defines basin geometry and hydraulic conductivities for a weakly non-linear base reservoir ($\beta=1, X_1=100$)	$X, Q_{in}, time_step, error_basis, basin_char, gw_hyd, flow$	$X=\{L_b, W_b, \alpha, K_s, K_b, K_z\}$	$\phi = \sum_{t=day}^{end\ day} \psi(t)\omega(t)$ (<i>error_option</i> ='total')
<i>cal_basetable</i>	Specify parameters for base reservoir storage-discharge function	$X, basin_char, gw_hyd, Q_{mean}$	$X=\{X_1, K_b, \beta\}$	$\left \frac{-Q_{mean}}{S_{b1}} - R_{b1} \right + \left \frac{-Q_{thresh}}{S_{b2}} - R_{b2} \right $
<i>cal_base</i>	Optimize base and vertical hydraulic conductivities	$X, Q_{in}, time_step, error_basis, basin_char, gw_hyd, flow$	$X=\{X_1, \beta, K_b, K_z\}$	$\phi = \sum_{t=day}^{end\ day} \psi(t)\omega(t)$ (<i>error_option</i> ='base')
<i>cal_surface</i>	Optimizes parameters for the sum of surface and baseflow	$X, Q_{in}, timestep, error_basis, basin_char, gw_hyd, flow$	$X=\{W_b, \alpha, K_s\}$	$\phi = \sum_{t=day}^{end\ day} \psi(t)\omega(t)$ (<i>error_option</i> ='total')

when $Q_b = Q_{thresh}$. This step only requires the utility function “base_table,” which creates a table with Z_b , S_b , and Q_b for discrete values of X_b from 0 to L_b . Calibration using “base_table” is more effective than directly calibrating base-reservoir parameters using *bf_sep*, which can converge on local minima in model error as a result of parameter values that generate minimal baseflow. The dynamic range in baseflow may still be limited by recharge, which only occurs between $X_b(t)$ (the intersection of the base water level and land surface) and L_b (the upper end of the stream basin).

The objective for the second calibration step is to find parameters for the base reservoir so that the recession rate is R_{b1} when $Q_b(t) = Q_{mean}$ and R_{b2} when $Q_b(t) = Q_{thresh}$, or minimization of:

$$\left| 1 - \frac{\left(\frac{-Q_{mean}}{S_{b1}} \right)}{R_{b1}} \right| + \left| 1 - \frac{R_{b2}}{\frac{-Q_{thresh}}{S_{b2}}} \right| \quad (24)$$

where

S_{b1} is base storage when $Q_b(t) = Q_{mean}$ and
 S_{b2} is base storage when $Q_b(t) = Q_{thresh}$.

The baseflow recession rate of the base reservoir can be sensitive to small changes in β and X_1 over a limited range of values.

In this case, optimization using the function *optim* may converge on parameter values that produce a local rather than global minimum in the objective. To force a wider search for values of β and X_1 , the objective is calculated from the storage values generated by *base_table* for a combinations of the parameters β and X_1 directly rather than using *optim*. The combinations span all values of β from 1 to 20 by increments of 0.1. For each value of β , X_1 is set to the maximum that permits $Q_b = Q_{mean}$. At this value of X_1 , the base reservoir must be fully saturated ($X_b = L_b$) for $Q_b = Q_{mean}$ and otherwise $Q_b < Q_{mean}$. The objective is calculated for the maximum value of X_1 that allows $Q_b = Q_{mean}$ and, then X_1 is decreased incrementally by 0.1 percent (0.001) while keeping β constant, which increases the saturated thickness of the base reservoir and its gradient at any value of X_b . Likewise, the curvature in the base reservoir surface moves downstream as X_1 decreases. The optimal value for X_1 generally will be close to the maximum value of X_1 so that the elevation of water surface in the base reservoir decreases rapidly when $Q_b \sim Q_{mean}$ and slowly when $Q_b \sim Q_{thresh}$.

Steps 3 and 4. Calibration of *bf_sep* for Baseflow Error and Total Error

Once the base storage-discharge relation (eq. 4) has been calibrated, the third calibration step optimizes X_1 , W_b , K_b , and K_z for baseflow error (*error_basis* = “base”).

This step effectively maximizes the baseflow component of streamflow. In the final calibration step, W_b , α , and K_s are calibrated to minimize the combined error of baseflow and surface flow (*error_basis* = “total”). The sequential calibration of parameters generally maximizes baseflow without over-simulating streamflow, avoids solutions where the baseflow component is a steady and small fraction of streamflow, but does not necessarily find a global minimum for total error.

Calibration of Multiple Sites

The model can be calibrated for multiple sites using the script *bf_sep_calibration.R*. The script reads site identification numbers, drainage areas, and streamflow data from local files or National Water Information System (NWIS; U.S. Geological Survey, 2022). It runs the four-step calibration process, writes the simulated time series to files, compiles parameter values, and summarizes the fraction of each flow components for each site. The script also creates a hydrograph for each site and saves it as a portable document format (.PDF) or image file format (.TIFF) to facilitate inspection of results. The script requires a control file that specifies a project name, the location of workspaces with the model functions, the location and name of the file with site identification numbers and drainage areas, the location of streamflow data (text file, an R object in a workspace, or NWIS web), the directory where output will be saved, the period of analysis, the time step, and the file format for saving hydrographs (.PDF or .TIFF). The directory receiving output should have the same name as the project, which will be appended to the beginning of each output file. In addition to saving output for individual sites, the script will compile parameters and summarize the baseflow fraction of streamflow for all sites into two respective files—*bf_params.csv* and *bff.csv*.

Base-Flow Simulations

BFS was calibrated at 13,208 USGS streamgages using available daily streamflow records for water years 1981 to 2020 (Konrad, 2020; fig. 3). The median simulated baseflow fraction (BFF) was 0.33. The median mean weighted absolute percent error was 0.05 (90 percent confidence interval [CI] of 0.01 to 0.18). The calibration process was generally successful at producing gradually declining baseflow that increased episodically in response to recharge events (rainfall or snowmelt) (fig. 4). Calibration was poor particularly at sites where extreme low flows occurred abruptly rather after a period of gradually receding streamflow. These sites are often downstream from reservoirs, tidally influenced, in streams that can freeze, or in non-perennial streams. An abrupt decrease in streamflow may also result from an equipment malfunction.

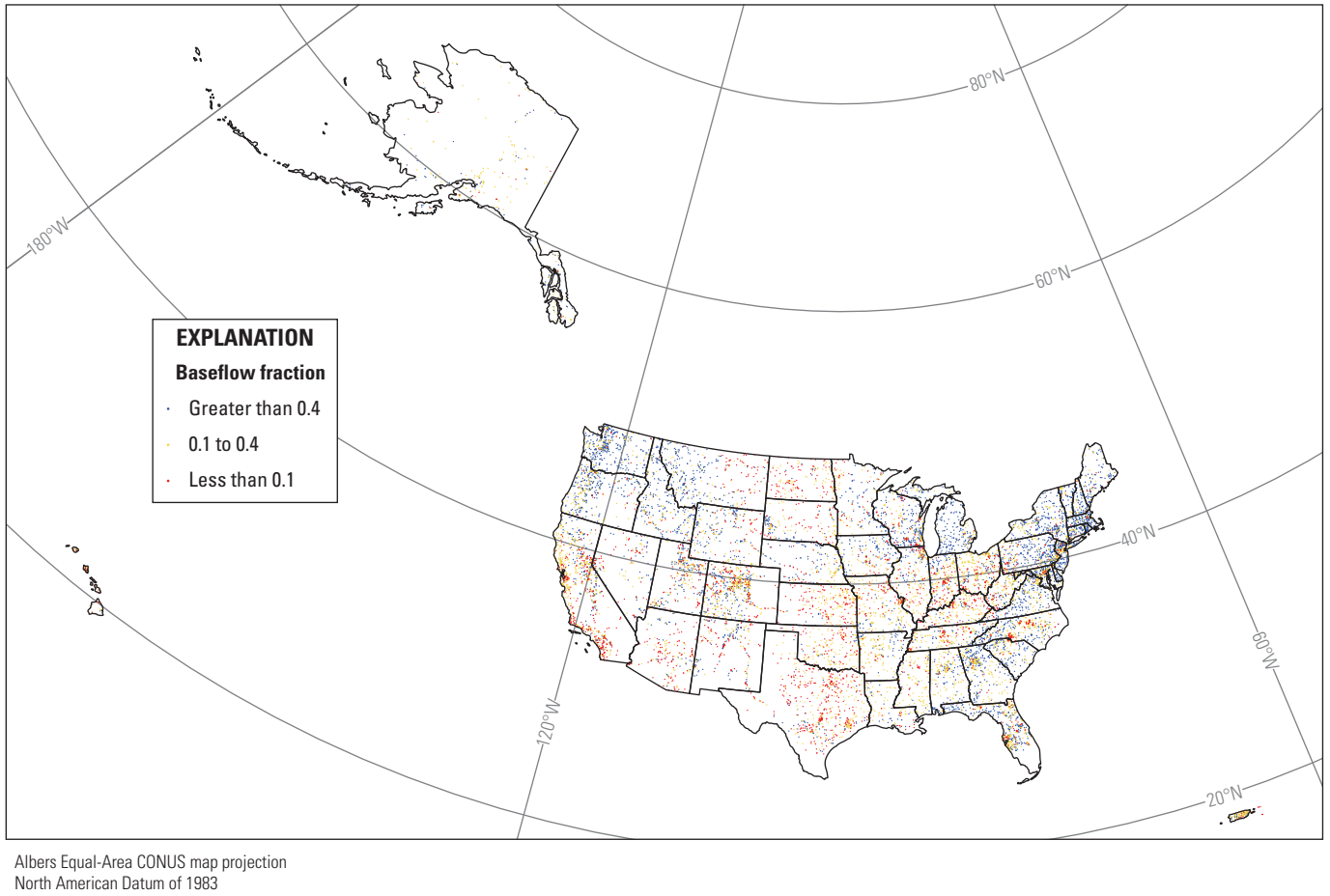


Figure 3. United States with the simulated baseflow fraction for 13,208 sites where the baseflow separation model was calibrated.

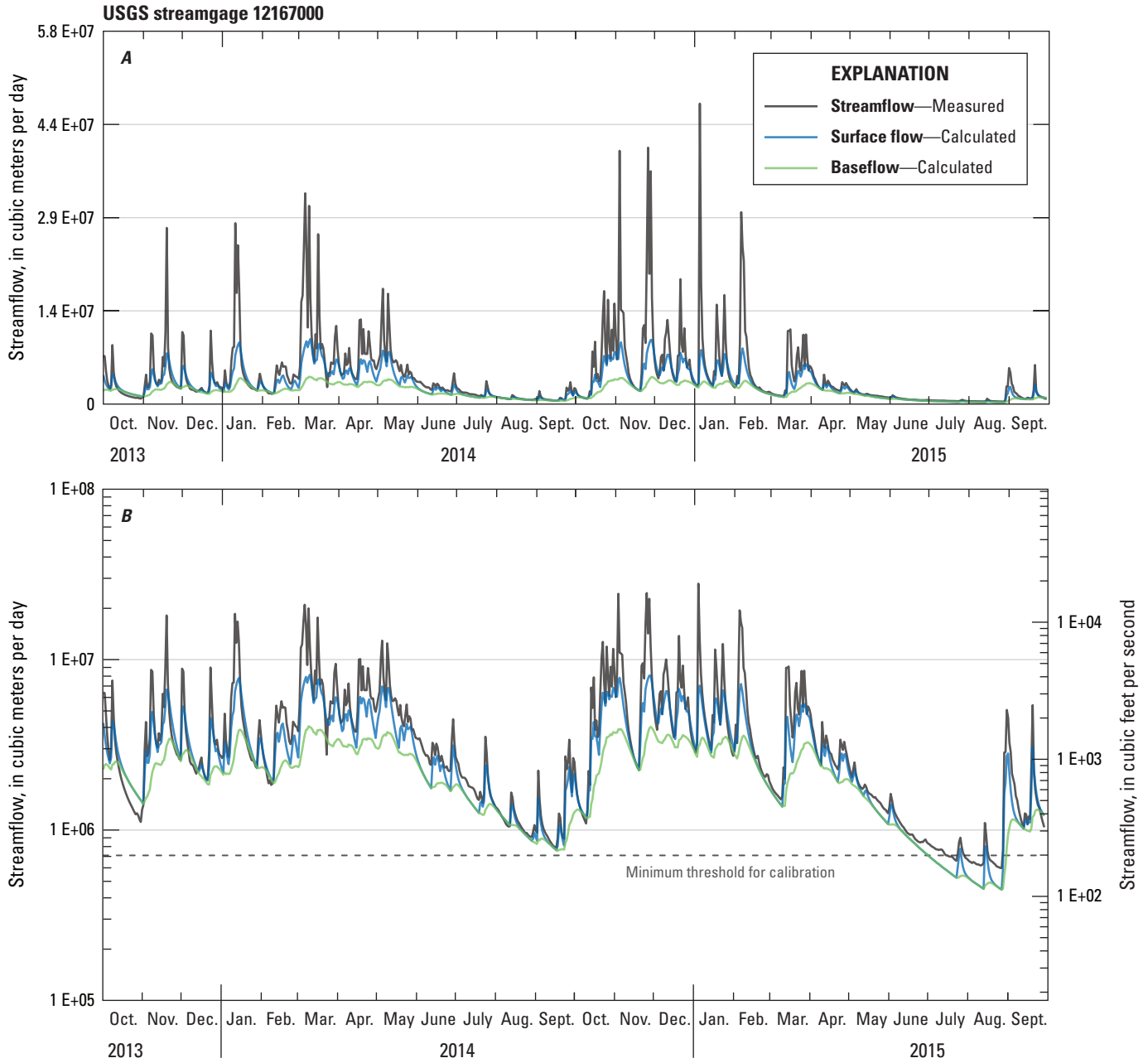


Figure 4. Observed daily streamflow, simulated baseflow, and the sum of simulated surface and baseflow calibrated model output for the North Fork Stillaguamish River (USGS streamgage No. 12167000; U.S. Geological Survey, 2022), water years 2014–15.

Comparison of Base-Flow Simulation to Graphical Hydrograph Separation

BFF was compared to the baseflow index (BFI) calculated using the Institute of Hydrology baseflow index for 8,368 sites in the continental United States (CONUS) (Wieczorek and others, 2018). BFF generally is less than BFI (median difference $BFF - BFI = -0.11$, 90 percent confidence interval of $-0.52, -0.08$) (fig. 5). Relatively large differences between BFF and BFI are pervasive for sites in the Interior West. Differences between BFF and BFI do not vary substantially with basin area (fig. 6).

Differences between BFI and BFF do not necessarily indicate errors in either approach because baseflow does not have a single definition but can be used to evaluate which methods are appropriate for specific applications. Three types of sites accounted for many of the large discrepancies between BFF and BFI in CONUS: (1) sites downstream from large reservoirs that regulate streamflow; (2) those with high elevation basins where snowmelt is a dominant mechanism generating runoff; and (3) other sites that have isolated, extremely low flows, as a result of stream drying or freezing for example.

Baseflow as a fraction of observed streamflow (BFF) is systematically less than BFI in regulated rivers. For 7,461 sites where normal reservoir storage was available from the 2013 National Inventory of Dams (Wieczorek and others, 2018), the median difference between BFF and BFI ranges from -0.06 for sites where reservoir storage is less than 1 day of mean streamflow to -0.26 for sites where reservoir storage is more than 100 days of mean streamflow (fig. 7). Steady releases from reservoirs and abrupt changes in streamflow during low-flow periods force calibration of BFS to solutions with low baseflow whereas BFI assigns more of the water released from a reservoir to baseflow.

Basin elevation accounts for differences between BFF and BFI, which ranges from -0.06 for low elevation basins to -0.44 for high elevation basins (fig. 8). In many cases, BFI includes snowmelt as part of baseflow whereas BFS may assign snowmelt to the surface flow fraction, SFF, of streamflow rather than the baseflow fraction. In these cases, $BFF + SFF$ may be closer to BFI.

A third category of sites with large discrepancies between BFF and BFI have extremely low values of streamflow that do not follow a gradual recession of streamflow. As with regulated rivers, calibration using a record that has abrupt decreases in streamflow forces baseflow down to the local minimum value and the model can only simulate a gradual recession to that local minimum.

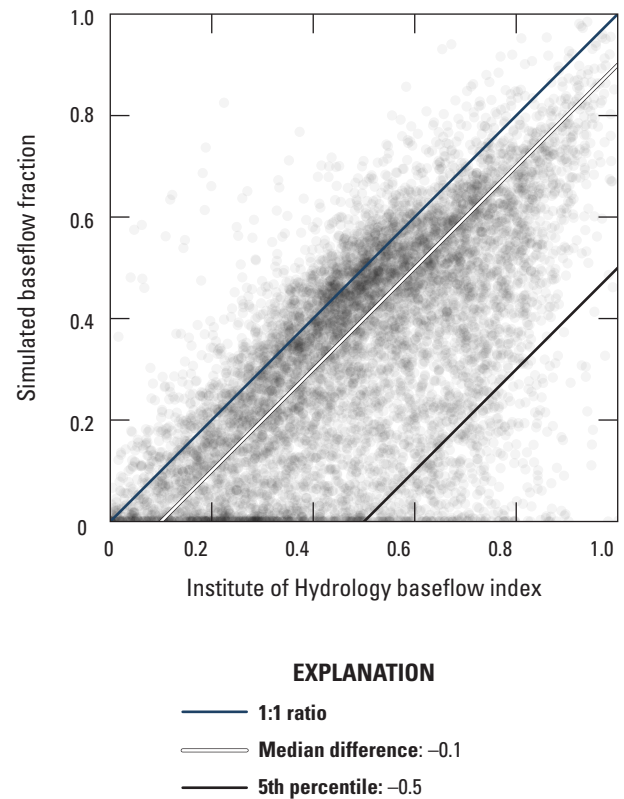


Figure 5. Comparison of the baseflow index to the simulated baseflow fraction of streamflow for 8,368 sites with streamgages operated by the U.S. Geological Survey (U.S. Geological Survey, 2022).

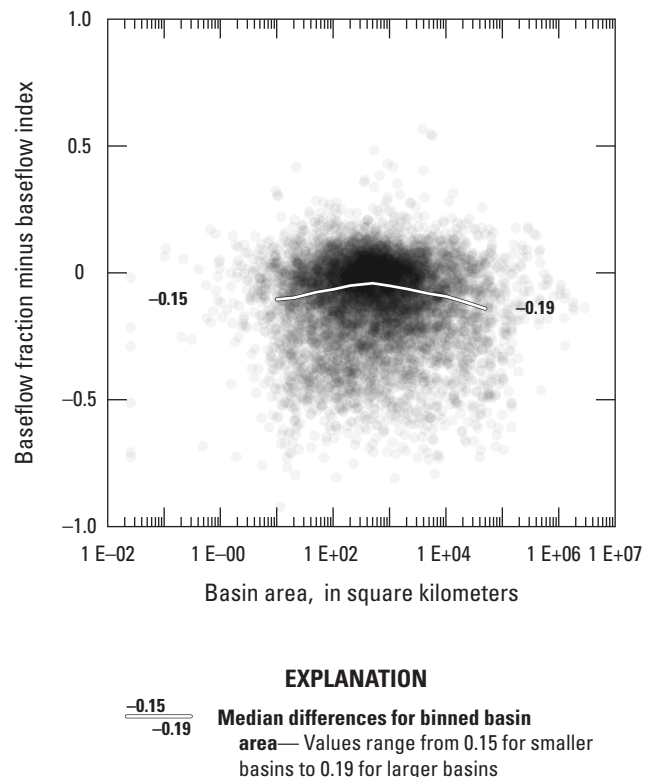
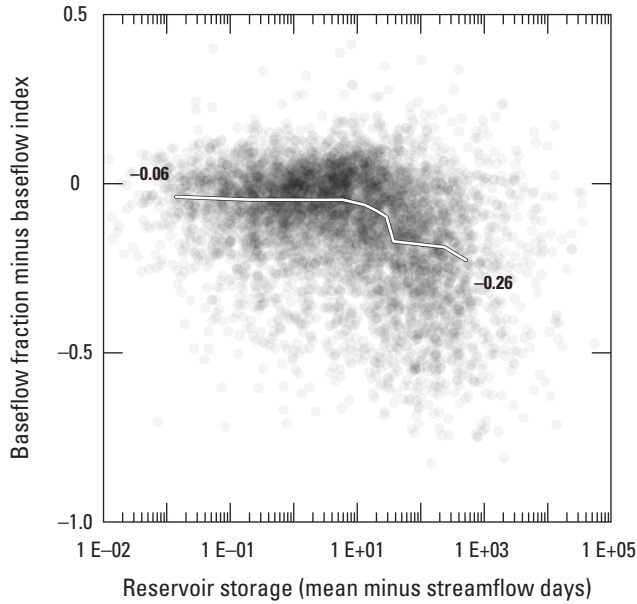


Figure 6. Difference between baseflow fraction and baseflow index in relation to basin area.



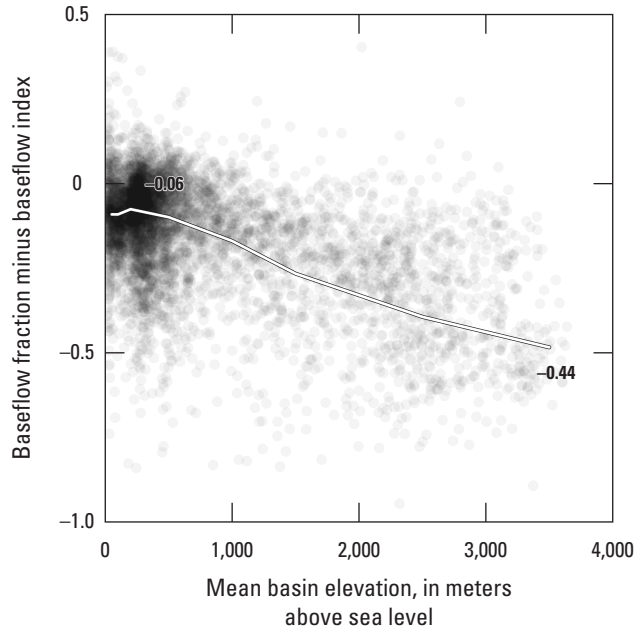
EXPLANATION
 Median differences for binned reservoir storage—
 Values range from 0.06 for basins with low reservoir storage to 0.26 for basins with high reservoir storage

Figure 7. Graph showing difference between baseflow fraction and baseflow index in relation to reservoir storage for 7,461 sites where data are available (2,409 sites with less than 0.001 day of storage are not shown).

Low-Flow Prediction and Forecasting

The unmeasured storage terms of a state-space model gives it the capacity to predict streamflow, unlike graphical or mixture-model methods for hydrograph separation, for periods with no rainfall or snowmelt. BFS uses storage at the end of periods with measured streamflow to calculate baseflow for periods without measured streamflow, which are designated by a value of NA for days missing measured streamflow. By appending future dates with streamflow equal to NA to the end of a record of measured streamflow, BFS will forecast baseflow assuming that there is no rainfall or snowmelt that infiltrates into the surface reservoir during the forecast period. The forecast can extend as far into the future as the user chooses, but the probability of the forecast decreases each day as the probability of no rainfall or snowmelt decreases.

The probability of the forecasted streamflow is a function of both model error, which can be estimated using the confidence interval of prediction and the probability of persistent dry condition, which decreases over time, and model error. When the probability of persistent dry conditions is close to 1 (a period with a dry meteorological forecast during a dry season), the uncertainty in forecasted streamflow would primarily be model error. As the probability of persistent dry conditions decreases over the forecast period, the likelihood



EXPLANATION
 Median differences for binned basin elevations—
 Values range from 0.06 for low elevation basins to 0.44 for high elevation basins

Figure 8. Difference between baseflow fraction and baseflow index in relation to mean basin elevation for 5,794 sites where upstream reservoir storage is less than 100 days of mean streamflow.

of a streamflow forecast from the baseflow separation model will decrease because streamflow is increasingly likely to have a surface-flow component and baseflow may increase in response to recharge. The likelihood of that dry conditions will persistent into the future can rapidly approach 0 in humid environments and during wet seasons (the probability that dry conditions will persist more than a few days is low). Because the baseflow forecast has a shifting probability over the forecast period, it is not directly comparable to forecasts with a constant probability, but it represents a “worst-case” scenario of minimum streamflow, which may be useful for drought-risk management.

The capability of the calibrated baseflow separation model for streamflow forecasting was evaluated using ψ (difference between baseflow and measured streamflow plus low-flow precision as a fraction of measured streamflow plus low-flow precision, eq. 18) for the last day, d , of each of the longest recession period with positive streamflow each year. There were 239,831 site-years with a mean of 18.2 annual values for the 13,208 sites where BFS has been calibrated. Median annual values were $\psi < 0.4$ for the last day of the longest recession period for 50 percent of the sites and $\psi < 1$ for the last day of the longest recession period for 90 percent of the sites. Sites with the highest 10 percent of median annual values of ψ were widely distributed but more likely in some regions including the central CONUS, Florida, southern California, and northern Alaska (fig. 9).

Large errors at some sites are likely a result of a short period of record for calibration, humid climates where low flows have an appreciable surface-flow component, or low-flow dynamics where first-order recession rates increase as streamflow decreases (because of stream drying or freezing for example). The results were filtered for 7,546 sites with at least 10 years of record and where normal reservoir storage was less than 100 days of mean streamflow and the median annual longest recession period is at least 10 days. The median annual error of forecasts on the day of longest recession was

0.4 for the median site. At these sites, model error is slightly lower for longer recession periods (fig. 10), indicating that forecast error does not increase over time during dry periods.

Streamflow forecasts with relatively large errors are typically biased down (under-predicting measured streamflow as shown in figs. 3 and 10). The bias in forecasting can be reduced by initializing the model using observed conditions immediately prior to the forecast period or adjusting for bias by forecasting current conditions and subtracting the current error as a percentage from the forecast for future time steps.

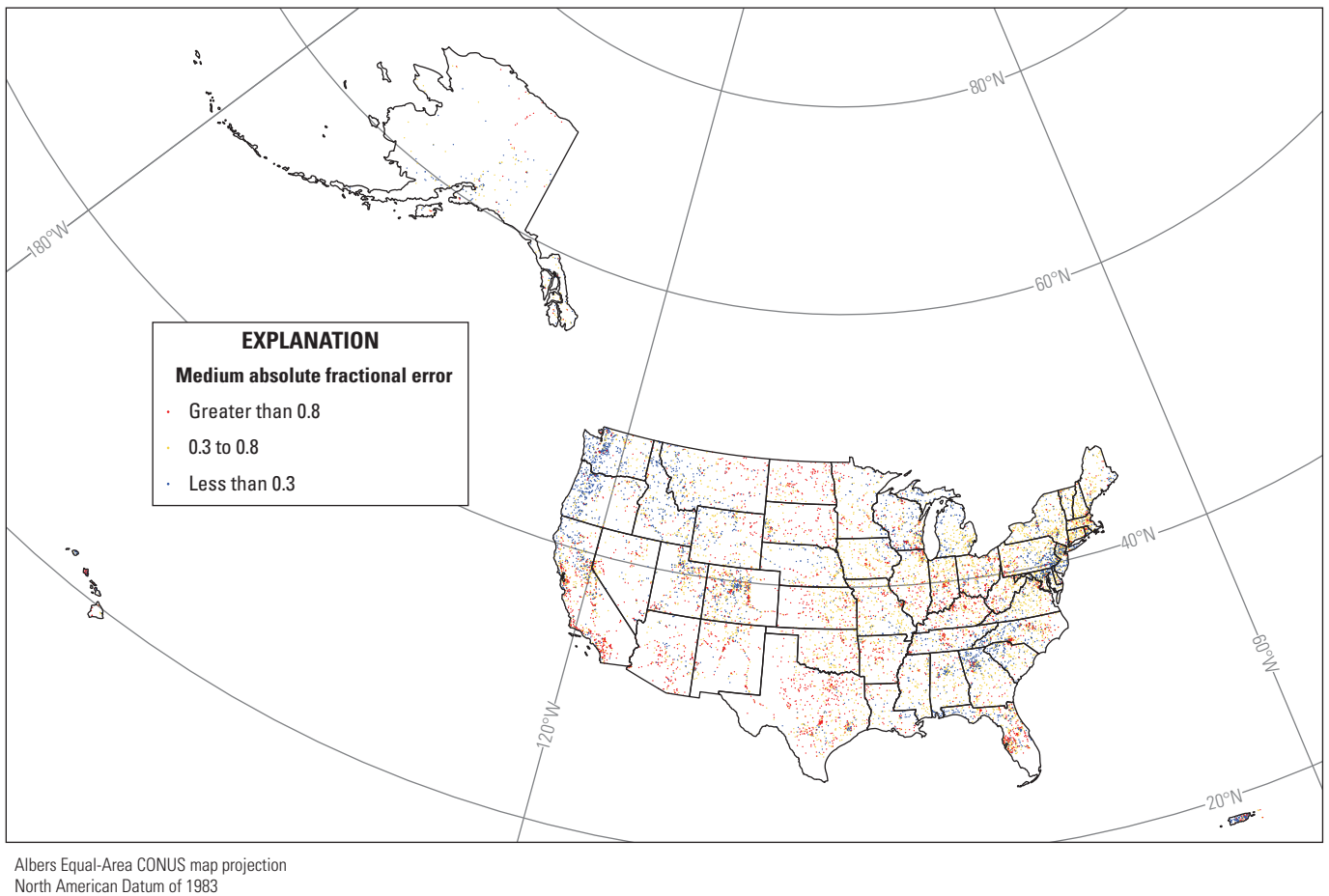


Figure 9. Median annual absolute fractional error for streamflow on the day of the annual longest recession period at 13,208 sites.

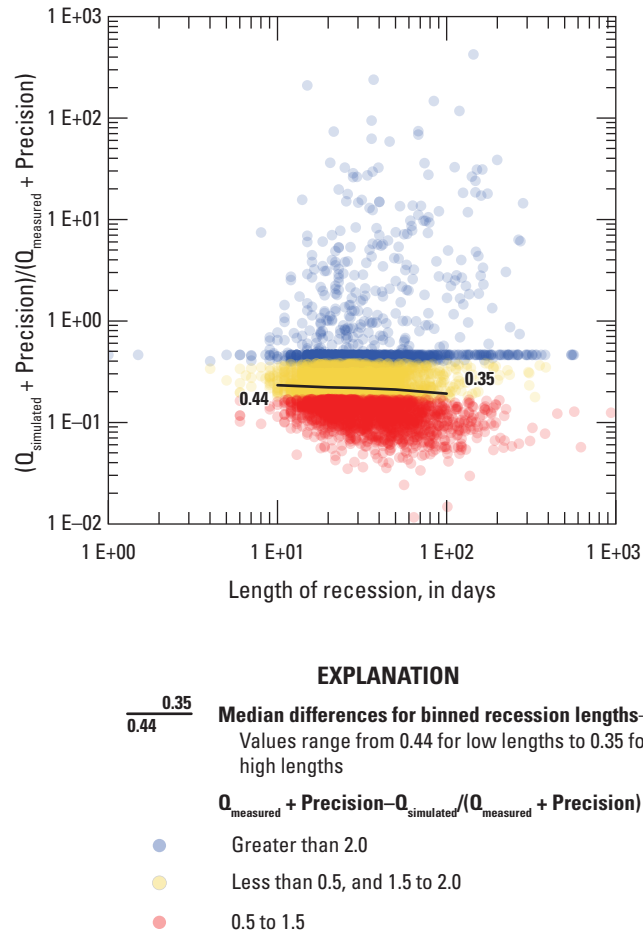


Figure 10. Median annual simulated streamflow plus precision as a fraction of measured streamflow plus precision ($Q_{\text{simulated}} + \text{Precision} / (Q_{\text{measured}} + \text{Precision})$) on the last day of annual longest recession plotted against the length of the recession period at 7,546 sites with at least 10 years of daily streamflow record where reservoir storage is less than 100 days of mean streamflow and the median annual longest recession period is at least 10 days.

Summary

A state-space model for baseflow separation, BFS, was developed and calibrated at 13,208 sites where the U.S. Geological Survey operated streamgages using available daily streamflow records from water years 1981 and 2020. The model simulates the baseflow component of streamflow as discharge from a base reservoir where discharge varies over time as a first-order, non-linear function of storage. The model calculates three components of streamflow—baseflow, surface

flow, and direct runoff. Baseflow represents groundwater discharge from a shallow aquifer into a stream channel, meltwater from glaciers and snowfields, relatively steady discharge from lakes and reservoirs, and streamflow with long transient times. Surface flow represents runoff from hillslope soils and snowmelt (surface reservoir). Direct runoff represents saturation overland flow during rain events or snowmelt.

The model generates impulses of water (rain or snowmelt) during time steps when streamflow increases. The impulses produce direct runoff from areas where the surface reservoir is fully saturated and infiltration where the surface reservoir has capacity available to store water. The surface reservoir discharges to the stream and recharges the base reservoir. Recharge is limited to areas above the unsaturated portion of the base reservoir. Flow through the reservoirs is assumed to be vertical for infiltration and recharge and horizontal for surface flow and baseflow. The direction of surface flow is lateral (perpendicular to the stream) and the direction of baseflow is longitudinal (parallel to the stream). The stream is assumed to drain all water in the base reservoir above the elevation of the channel, so the model does not resolve the curvature of local groundwater flow paths from a longitudinal to a lateral direction, which can be expected around a stream channel.

Model calibration is challenged by the lack of an independent measure of baseflow, non-linear discharge-storage function for the base reservoir, and an objective that baseflow varies over time but does not exceed streamflow. The model has three features to facilitate calibration—errors weighted by the length of recession (time since an increase in streamflow) for a time step; incorporation of low-flow measurement precision in the error calculations; and a minimum threshold streamflow for calculating errors to filter out measurement noise and time steps when first-order recession rates increase as streamflow decreases.

The model can forecast streamflow for dry periods at sites with real-time gaging by specifying measured streamflow as Not Available (NA) for the period. The probability of the forecast decreases each day in the future as the cumulative probability of dry weather decreases over the forecast period. The confidence intervals of prediction should be examined for any site where the model is used for forecasting. The median annual fractional error for streamflow at end of the longest recession period each year was 0.4 for sites with at least 10 years of record. Forecasts from BFS were generally less than measured streamflow and the error was often a consistent percentage of measured flow during any recession period, which may allow for bias correction as part of forecasting.

References Cited

- Botter, G., Porporato, A., Rodriguez-Iturbe, I., and Rinaldo, A., 2009, Nonlinear storage-discharge relations and catchment streamflow regimes: *Water Resources Research*, v. 45, no. 10, W10427., accessed May 18, 2021, at <https://doi.org/10.1029/2008WR007658>.
- Clark, M.P., Rupp, D.E., Woods, R.A., Zheng, X. Ibbitt, R.P., Slater, A.G., Schmidt, J., Uddstrom, M.J., 2008, Hydrological data assimilation with the ensemble Kalman filter: Use of streamflow observations to update states in a distributed hydrological model: *Advances in Water Resources*, v. 31, no. 10, p. 1309–1324, accessed March 25, 2019, at <https://doi.org/10.1016/j.advwatres.2008.06.005>.
- Clark, M.P., and Kavetski, D., 2010, Ancient numerical daemons of conceptual hydrological modeling—1. Fidelity and efficiency of time stepping schemes: *Water Resources Research*, v. 46, no. 10, W10510, accessed April 5, 2019, at <https://doi.org/10.1029/2009WR008894>.
- Curtis, J.A., Burns, E.R., and Sando, R., 2020, Regional patterns in hydrologic response, a new three-component metric for hydrograph analysis and implications for ecohydrology, Northwest Volcanic Aquifer Study Area, USA: *Journal of Hydrology. Regional Studies*, v. 30, p. 100698, accessed June 22, 2020, at <https://doi.org/10.1016/j.ejrh.2020.100698>.
- Dooge, J.C.I., 1959, A general theory of the unit hydrograph: *Journal of Geophysical Research*, v. 64, no. 2, p. 241–256, accessed March 25, 2019, at <https://doi.org/10.1029/JZ064i002p00241>.
- Duan, Q., Sorooshian, S., and Gupta, V., 1992, Effective and efficient global optimization for conceptual rainfall-runoff models: *Water Resources Research*, v. 28, no. 4, p. 1015–1031, accessed February 3, 2019, at <https://doi.org/10.1029/91WR02985>.
- Durbin, J., and Koopman, S.J., 2012, *Time series analysis by State Space Models*: Oxford, Oxford University Press, 346 p.
- Freeze, R.A., and Cherry, J.A., 1979, *Groundwater*: Englewood Cliffs, NJ, Prentice-Hall, 604 p.
- Gochis, D.J., Barlage, M., Cabell, R., Casali, M., Dugger, A., FitzGerald, K., McAllister, M., McCreight, J., Rafieei Nasab, A., Read, L., Sampson, K., Yates, D., and Zhang, Y., 2020, The WRF-Hydro modeling system technical description, Version 5.1.1, NCAR Technical Note, 107 p., accessed November 20, 2020, at https://ral.ucar.edu/sites/default/files/public/projects/wrf_hydro/technical-description-user-guide/wrf-hydro-v5.1.1-technical-description.pdf.
- Jakeman, A.J., Littlewood, I.G., and Whitehead, P.G., 1990, Computation of the instantaneous unit hydrograph and identifiable component flows with application to two small upland catchments: *Journal of Hydrology*, v. 117, nos. 1–4, p. 275–300, accessed March 12, 2019, at [https://doi.org/10.1016/0022-1694\(90\)90097-H](https://doi.org/10.1016/0022-1694(90)90097-H).
- Kavetski, D., and Kuczera, G., 2007, Model smoothing strategies to remove microscale discontinuities and spurious secondary optima in objective functions in hydrological calibration: *Water Resources Research*, v. 43, no. 3, W03411, accessed November 19, 2020, at <https://doi.org/10.1029/2006WR005195>.
- Kirchner, J.W., 2009, Catchments as simple dynamical systems—Catchment characterization, rainfall-runoff modeling, and doing hydrology backward: *Water Resources Research*, v. 45, no. 2, W02429, accessed December 7, 2020, at <https://doi.org/10.1029/2008WR006912>.
- Konrad, C.P., 2006a, Longitudinal hydraulic analysis of river-aquifer exchanges: *Water Resources Research*, v. 42, no. 8, W08425, accessed August 21, 2006, at <https://doi.org/10.1029/2005WR004197>.
- Konrad, C.P., 2006b, Location and timing of river-aquifer exchanges in six tributaries to the Columbia River in the Pacific Northwest of the United States: *Journal of Hydrology*, v. 329, nos. 3–4, p. 444–470, accessed September 27, 2006, at <https://doi.org/10.1016/j.jhydrol.2006.02.028>.
- Konrad, C.P., 2020, Non-linear baseflow separation model with parameters and results (ver. 2.0, October 2022): U.S. Geological Survey data release, accessed October 26, 2022, at <https://doi.org/10.5066/P9AIPHEP>.
- Linsley, R.K., Kohler, M.A., and Paulhus, J.L.H., 1982, *Hydrology for Engineers*: New York, McGraw Hill, 508 p.
- Mahler, B.J., Nowell, L.H., Sandstrom, M.W., Bradley, P.M., Romanok, K.M., Konrad, C.P., and Van Metre, P.C, 2021, Inclusion of pesticide transformation products is key to estimating pesticide exposures and effects in small U.S. streams: *Environmental Science & Technology*, v. 55, no. 8, p. 4740–4752, accessed May 24, 2022, at <https://doi.org/10.1021/acs.est.0c06625>.
- Miller, M.P., Susong, D.D., Shope, C.L., Heilweil, V.M., and Stolp, B.J., 2014, Continuous estimation of baseflow in snowmelt-dominated streams and rivers in the Upper Colorado River Basin—A chemical hydrograph separation approach: *Water Resources Research*, v. 50, no. 8, p. 6986–6999, accessed December 3, 2018, at <https://doi.org/10.1002/2013WR014939>.

- Nathan, R.J., and McMahon, T.A., 1990, Evaluation of automated techniques for base flow and recession analysis: *Water Resources Research*, v. 26, no. 7, p. 1465–1473, accessed September 2, 2020, at <https://doi.org/10.1029/WR026i007p01465>.
- Neitsch, S.L., Arnold, J.G., Kiniry, J.R., and Williams, J.R., 2011, Soil and Water Assessment Tool, Theoretical Documentation, version 2009: Texas Water Resources Institute Technical Report 406, Texas A & M University, College Station, Texas.
- Potter, S.T., and Gburek, W.J., 1986, Simulation of the seepage face—Limitations of a one-dimensional approach: *Journal of Hydrology*, v. 87, nos. 3–4, p. 379–394, [https://doi.org/10.1016/0022-1694\(86\)90025-9](https://doi.org/10.1016/0022-1694(86)90025-9).
- R Core Team, 2020a, R language for statistical computing, version 4.0.3, released October 10, 2020.
- R Core Team, 2020b, Stats package: The Comprehensive R Archive Network web page, accessed October 10, 2020, at cran.r-project.org.
- Raffensperger, J.P., Baker, A.C., Blomquist, J.D., and Hopple, J.A., 2017a, Optimal hydrograph separation using a recursive digital filter constrained by chemical mass balance, with application to selected Chesapeake Bay watersheds: U.S. Geological Survey Scientific Investigations Report 2017–5034, 51 p., accessed July 29, 2020, at <https://doi.org/10.3133/sir20175034>.
- Regan, R.S., Markstrom, S.L., Hay, L.E., Viger, R.J., Norton, P.A., Driscoll, J.M., and LaFontaine, J.H., 2018, Description of the National Hydrologic Model for use with the Precipitation-Runoff Modeling System (PRMS): U.S. Geological Survey Techniques and Methods, book 6, chap B9, 38 p., accessed May 13, 2020, at <https://doi.org/10.3133/tm6B9>.
- Rutledge, A.T., 1998, Computer programs for describing the recession of ground-water discharge and for estimating mean ground-water recharge and discharge from streamflow records - update: U.S. Geological Survey Water-Resources Investigations Report 98–4148, 43 p.
- Serrano, S.E., and Workman, S.R., 1998, Modeling transient stream/aquifer interaction with the non-linear Boussinesq equation and its analytical solution: *Journal of Hydrology*, v. 206, nos. 3–4, p. 245–255, accessed November 6, 2020, at [https://doi.org/10.1016/S0022-1694\(98\)00111-5](https://doi.org/10.1016/S0022-1694(98)00111-5).
- Sloto, R.A., and Crouse, M.Y., 1996, HYSEP—A computer program for streamflow hydrograph separation and analysis: U.S. Geological Survey Water-Resources Investigations Report 96–4040, 46 p.
- Stewart, M., Cimino, J., and Ross, M., 2007, Calibration of base flow separation methods with streamflow conductivity: *Ground Water*, v. 45, no. 1, p. 17–27, accessed June 28, 2020, at <https://doi.org/10.1111/j.1745-6584.2006.00263.x>.
- Stewart, M.K., and McDonnell, J.J., 1991, Modeling base flow soil water residence times from deuterium concentrations: *Water Resources Research*, v. 27, no. 10, p. 2681–2693, accessed February 12, 2020, at <https://doi.org/10.1029/91WR01569>.
- Tallaksen, L.M., 1995, A review of baseflow recession analysis: *Journal of Hydrology*, v. 165, nos. 1–4, p. 349–370, accessed November 15, 2020, at [https://doi.org/10.1016/0022-1694\(94\)02540-R](https://doi.org/10.1016/0022-1694(94)02540-R).
- U.S. Geological Survey, 2022, National Water Information System: U.S. Geological Survey web interface, <https://doi.org/10.5066/F7P55KJN>, accessed October 27, 2021 at <https://nwis.waterdata.usgs.gov/nwis>.
- Wieczorek, M.E., Jackson, S.E., and Schwarz, G.E., 2018, Select attributes for NHDPlus version 2.1 reach catchments and modified network routed upstream watersheds for the conterminous United States (ver. 2.0, November 2019): U.S. Geological Survey data release, accessed February 3, 2020, at <https://doi.org/10.5066/F7765D7V>.
- Wittenberg, H., 1999, Baseflow recession and recharge as nonlinear storage processes: *Hydrological Processes*, v. 13, no. 5, p. 715–726, [https://onlinelibrary.wiley.com/doi/10.1002/\(SICI\)1099-1085\(19990415\)13:5%3C715::AID-HYP775%3E3.0.CO;2-N](https://onlinelibrary.wiley.com/doi/10.1002/(SICI)1099-1085(19990415)13:5%3C715::AID-HYP775%3E3.0.CO;2-N).

For information about the research in this report, contact
Director, Washington Water Science Center
U.S. Geological Survey
934 Broadway, Suite 300
Tacoma, Washington 98402
<https://www.usgs.gov/centers/washington-water-science-center>

Manuscript approved on October 26, 2022

Publishing support provided by the U.S. Geological Survey
Science Publishing Network, Tacoma Publishing Service Center

